

DESIGN OF A BELLOW ACTUATOR INSPIRED BY THE SQUID LOCOMOTION



by
Oğuzhan Kaya

Submitted to Graduate School of Natural and Applied Sciences
in Partial Fulfillment of the Requirements
for the Degree of Master of Science in
Mechanical Engineering

Yeditepe University
2017

DESIGN OF A BELLOW ACTUATOR INSPIRED BY THE SQUID LOCOMOTION

APPROVED BY:

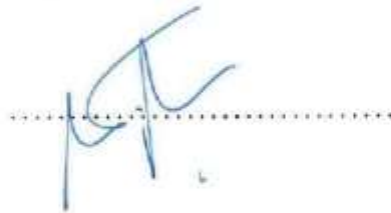
Assist. Prof. Dr. Onur Cem Namlı
(Thesis Supervisor)



Assist. Prof. Dr. Ali Bahadır Olcay



Assist. Prof. Dr. Mehmet Gökhan Gökçen



DATE OF APPROVAL: / / 2017

ACKNOWLEDGEMENTS

I would like to express my very great appreciation to my advisor Yrd. Doc. Dr. Onur Cem Namlı and Yrd. Doc. Dr. Bahadır Olcay. His sensible advices enable me to cope with critical points.

Also, I would like to thank to Yeditepe University and Department of Mechanical Engineering for education and opportunity to complete my master degree.

Lastly, I would like to thank to my family and my girlfriend with their endless support.

ABSTRACT

DESIGNING OF A BELLOW ACTUATOR INSPIRED BY THE SQUID LOCOMOTION

Squids, members of the cephalopods, are known to be the fastest swimmers in aquatic invertebrates because of their unique swimming performance under water. The swimming technique of a squid is quite different when compared with other aquatic creatures. Squids typically produce powerful jets by impulsively ejecting the water initially in their mantle cavity. Therefore, a mantle cavity of a squid plays a key role when a mantle wall tissue applies a significant pressure to the water inside the mantle cavity prior to accelerate.

The purpose of the present study is to identify the mechanical properties of mantle wall tissue made from an organic composite composed of circular, radial muscles and designing squid mantle cavity analytically. The results of the tensile test indicated that mean elastic moduli of the mantle tissue ranged from 500 to 900 kPa while shear modulus values for the tissue varied from 11 to 15kPa. Besides, a compression test showed that the Poisson's ratio was about 0.34 for the tissue and microscopic tissue analysis showed that the volume fraction ratio of the radial muscles to circular (hoop) ones were 1 to 8.6.

Mechanical properties of squid mantle is used to create a composite squid mantle wall. Circular muscles and radial muscles' working structures are known and designed as real squid mantle wall.

Also, squid locomotion system experimental test setup are made. As a squid mantle wall, bellow is used. Shape memory alloys and steel springs are used. Steel springs used to compress the bellow and shape memory alloys make the test setup back to initial position to examine the propulsion.

ÖZET

KÖRÜK AKTÜATÖRÜ DİZAYNI KALAMAR HAREKET YETENEĞİNDEN İLHAM ALINARAK

Su altındaki yaşam her zaman birçok araştırmacının dikkatini uzun yıllardır çekmeyi başarmıştır. Özellikle, kalamarın su altındaki yüzme performansından esinlenerek bu çalışmada bir kalamarın saniyeden daha az bir sürede 30 - 40 km/h hıza çıkmayı nasıl başardığını anlamak amaçlanmıştır. Bir kalamarın yüzme tekniği diğer su altı canlıları ile karşılaştırıldığında oldukça farklıdır. Kalamarlar genelde başlangıçta karın boşluklarında bulunan suyu çok kısa zaman içerisinde püskürterek güçlü jetler oluştururlar. Böylece, karın dokusu duvarı karın boşluğundaki suya önemli bir basınç uyguladığı zaman bir kalamarın karın boşluğu önemli bir rol oynar.

Bu çalışmada, dairesel (çember) ve radyal kaslardan oluşan organik bir kompozit olan kalamar karın dokusunun elastik modülü, kayma modülü ve Poisson oranı tespit edilmiştir. Kalamar karın dokusunun mekanik özelliklerini bilmek ve kompozit modelini çıkarmak kalamarın yüzme stilini açıklamakta faydalı olacaktır. Çekme testi sonuçları, karın dokusunun elastik modülünü 500 ila 800 kPa arasında göstermektedir. Kesme modülü değerleri 11 ile 15 kPa arasında değişmektedir. Kısıtlı ve kısıtsız sıkıştırma testi sonucunda Poisson oranı yaklaşık 0.34 olarak tespit edilmiştir. Mikroskobik doku analizi radyal kasların dairesel (çember) kaslara oranını 1'e 12 olarak vererek kasların hacim fraksiyonu hakkında bilgi vermiştir.

Kalamar karın duvarının mekanik özelliklerinden faydalanarak birleşik bir kalamar karın duvarı dizaynı yapıldı. Dairesel ve radyal kas yapısı gerçek kalamardan öğrenildi ve birleşik kalamar dizaynında kullanıldı.

Ayrıca, kalamar hareket sistemine benzer bir test sistemi düzenlendi. Körük kalamar karnı olarak kullanılıyor. Deney düzeneğinde çelik yaylar ve şekillendirilebilir yaylar kullanılıyor. Çelik yaylar körüğü sıkmak için kullanılıyor, şekillendirilebilir yaylar ise çelik yayları çekip körüğü eski haline getirebilmek için kullanılıyor.

TABLE OF CONTENTS

ACKNOWLEDGEMENTS.....	iii
ABSTRACT.....	iv
ÖZET	v
LIST OF FIGURES	viii
LIST OF TABLES.....	xiii
LIST OF SYMBOLS/ABBREVIATIONS.....	xvi
1. INTRODUCTION.....	1
2. MATERIALS AND METHOD	5
3. SQUID MANTLE WALL MECHANICAL PROPERTIES	7
3.1. TENSILE TEST EXPERIMENT.....	7
3.2. SHEAR TEST EXPERIMENT.....	10
3.3. COMPRESSION TEST EXPERIMENT.....	12
3.4. SQUID MANTLE WALL WORKING PRINCIPLE.....	15
4. SQUID MANTLE WALL COMPOSITE DESIGN	17
5. SHAPE MEMORY BASED SQUID DESIGN	22
5.1. SHAPE MEMORY ALLOY HEATING.....	22
5.2. BELLOW COMPRESSION TENSION TEST	27
5.3. SOLENOID WORKING PRINCIPLE	29
6. SMOKE VISUALIZATION OF ACTUATOR BASED SQUID DESIGN WITH OR WITHOUT SHAPE MEMORY ALLOY.....	30
6.1. SMOKE VISUALIZATION WITHOUT SHAPE MEMORY ALLOY.....	30
6.2. MECHANICAL SQUID MANTLE CAVITY PROPULSION WITH SHAPE MEMORY ALLOY	40
7. RESULTS.....	53
7.1. EFFECT OF NOZZLE DIAMETER ON PROPULSION EFFICIENCY	53
7.2. EFFECT OF NOZZLE DIAMETER ON PROPULSION EFFICIENCY	56
7.3. EFFECT OF SPRING CONSTANT ON SMOKE PROPULSION	59

7.4. EFFECT OF NOZZLE DIAMETER PROPULSION EFFICIENCY WITH SHAPE MEMORY ALLOY.....	62
7.5. EFFECT OF SPRING DIAMETER ON PROPULSION EFFICIENCY WITH SHAPE MEMORY ALLOY.....	65
7.6. EFFECT OF NOZZLE DIAMETER ON SMOKE PROPULSION WITH SHAPE MEMORY ALLOY	68
7.7. EFFECT OF SPRING DIAMETER ON SMOKE PROPULSION WITH SHAPE MEMORY ALLOY	71
8. CONCLUSION	74
REFERENCES	77

LIST OF FIGURES

Figure 2.1. Jet cycle schema	5
Figure 2.2. Complete Model of Mechanical Squid Mantle Testing Device	6
Figure 3.1. Front and side view of circular specimen with tensile test.....	8
Figure 3.2. Diagram of a piece cut from the squid mantle wall	9
Figure 3.3. Stress/strain curves resulting from a single loading cycle of three different squid mantle tissue blocks	9
Figure 3.4. Front view of shear testing specimen	11
Figure 3.5. Shear stress strain behavior of the mantle wall tissue	12
Figure 3.6. Unconstrained and constrained compression test.....	13
Figure 3.7. Compression test results showing the stress strain relationship for constrained compression test and unconstrained compression test.....	14
Figure 3.8. Cross section of squid mantle cavity	16
Figure 3.9. Squid mantle wall circular and radial muscles relation.....	16
Figure 4.1. Micrographs of squid mantle shows circular and radial muscle arrangement ..	17
Figure 4.2. Squid nozzle diameter change	19

Figure 4.3. Squid mantle cavity composite structure front and side view	20
Figure 5.1. Diagram of shape memory alloy's microscopic structure	23
Figure 5.2. Shape memory alloy and steel spring	23
Figure 5.3. Shape memory alloy and steel spring movement length	24
Figure 5.4. Shape memory alloy applied voltage and measuring actuation temperature with thermocouple	25
Figure 5.5. Thermocouple measuring shape memory alloy actuation temperature	26
Figure 5.6. Bellow dimensions	27
Figure 5.7. Bellow compression by using instron testing device	28
Figure 5.8. Bellow compression and tension graph	28
Figure 5.9. Solenoid and Arduino working diagram	29
Figure 6.1. Smoke propulsion stages	32
Figure 6.2. Propulsion efficiency versus time 10 mm nozzle diameter 0.7 mm spring diameter	33
Figure 6.3. Propulsion stages	34
Figure 6.4. Smoke propulsion versus time 2.5 mm nozzle diameter and 0.9 mm spring diameter	35

Figure 6.5. Propulsion efficiency versus time 2.5 mm nozzle diameter and 0.9 mm spring diameter	36
Figure 6.6. Propulsion efficiency of 2.5 mm nozzle diameter and 0.7 mm spring diameter versus time	42
Figure 6.7. Propulsion speed versus time	42
Figure 6.8. 5 mm nozzle diameter and 0.9 mm spring diameter propulsion efficiency versus time	46
Figure 6.9. 5 mm nozzle diameter and 0.9 mm spring diameter propulsion speed versus time	47
Figure 6.10. 10 mm nozzle diameter and 0.9 mm spring diameter propulsion efficiency versus time	48
Figure 6.11. Propulsion efficiency of 5 mm diameter and 1 mm spring diameter versus time	50
Figure 6.12. Propulsion speed versus time	51
Figure 7.1. Propulsion efficiency versus time on 2.5 mm nozzle diameter with different spring constant	53

Figure 7.2. Propulsion efficiency versus time on 5 mm nozzle diameter with different spring constant 54

Figure 7.3. Propulsion efficiency versus time on 10 mm nozzle diameter with different spring constant 55

Figure 7.4. Propulsion efficiency versus time on 0.7 mm spring diameter with different nozzle diameter 56

Figure 7.5. Propulsion efficiency versus time on 0.9 mm spring diameter with different nozzle diameter 57

Figure 7.6. Propulsion efficiency versus time on 1 mm spring diameter with different nozzle diameter 58

Figure 7.7. Smoke propulsion versus time on 0.7 mm spring diameter with different nozzle diameters 59

Figure 7.8. Smoke propulsion versus time on 0.9 mm spring diameter with different nozzle diameter 60

Figure 7.9. Smoke propulsion versus time on 1 mm spring diameter with different nozzle diameter 61

Figure 7.10. Propulsion efficiency of 0.7 mm spring diameter versus time 62

Figure 7.11. Propulsion efficiency of 0.9 mm spring diameter versus time.....	63
Figure 7.12. Propulsion efficiency of 1 mm spring diameter versus time.....	64
Figure 7.13. Propulsion efficiency of 2.5 mm nozzle diameter versus time	65
Figure 7.14. Propulsion efficiency of 5 mm nozzle diameter versus time	66
Figure 7.15. Propulsion efficiency of 10 mm nozzle diameter versus time	67
Figure 7.16. Smoke propulsion of 0.7 mm spring diameter versus time	68
Figure 7.17. Smoke propulsion of 0.9 mm spring diameter	69
Figure 7.18. Smoke propulsion of 1 mm spring diameter	70
Figure 7.19. Smoke propulsion of 2.5 mm nozzle diameter versus time	71
Figure 7.20. Smoke propulsion of 5 mm nozzle diameter versus time	72
Figure 7.21. Smoke propulsion of 10 mm nozzle diameter versus time	73
Figure 8.1. Propulsion efficiencies of without and with SMA	76

LIST OF TABLES

Table 3.1. Measurements of the squid's geometrical dimensions	8
Table 3.2. Small sized-squid midsection and heading tensile test young's modulus results	10
Table 3.3. Thickness measurement and area calculaiton of top section and left section.....	11
Table 4.1. Mechanical propoerties of nitinol	17
Table 4.2. Squid mantle wall tissue	18
Table 4.3. Squid mantle cavity change by slow swimming and jet escape	19
Table 4.4. Elastomer and steel spring properties	20
Table 6.1. Camera settings.....	31
Table 6.2. 2.5 mm nozzle diameter and 0.7 mm spring diameter.....	31
Table 6.3. 5mm nozzle diameter and 0.7 mm spring diameter.....	32
Table 6.4. 10 mm nozzle diameter and 0.7 mm spring diameter.....	33
Table 6.5. 0.9 mm spring diameter and 2.5 mm nozzle diameter.....	35
Table 6.6. 5mm nozzle diameter and 0.9 mm spring diameter.....	37
Table 6.7. 10 mm nozzle diameter and 0.9 mm spring diameter.....	38

Table 6.8. 1mm spring diameter and 2.5 mm nozzle diameter.....	38
Table 6.9. 1 mm spring diameter and 5 mm nozzle diameter.....	39
Table 6.10. 10 mm nozzle diameter and 1 mm spring diameter.....	39
Table 6.11. Sma actuation observation and records	40
Table 6.12. 2.5 mm nozzle diameter and 0.7 mm spring diameter with shape memory alloy	41
Table 6.13. 5 mm nozzle diameter and 0.7 mm spring diameter with shape memory alloy	43
Table 6.14. 10 mm nozzle diameter and 0.7 mm spring diameter with shape memory alloy	44
Table 6.15. 2.5 mm nozzle diameter and 0.9 mm spring diameter with shape memory alloy	45
Table 6.16. 5 mm nozzle diameter and 0.9 mm spring diameter with shape memory alloy	46
Table 6.17. 10 mm nozzle diameter and 0.9 mm spring diameter with shape memory alloy	48
Table 6.18. 2.5 mm nozzle diameter and 1 mm spring diameter with shape memory alloy	49
Table 6.19. 5 mm nozzle diameter and 1 mm spring diameter.....	50
Table 6.20. 10 mm nozzle diameter and 1 mm spring diameter.....	52

Table 7.1. Starting propulsion efficiencies55



LIST OF SYMBOLS/ABBREVIATIONS

D	Diameter
E_b	Constrained young's modulus
E_c	Composite young's modulus
E_f	Fiber young's modulus
E_m	Matrix young's modulus
E_o	Unconstrained young's modulus
G	Modulus of rigidity
K	Spring constant
r	Radius
N	Spring constant
V_f	Fiber volume fraction
V_m	Matrix volume fraction
U_j	Smoke propulsion speed
V_m	Efficiency
V_m	Density
ν	Poisson's ration
τ	Shear stress

1. INTRODUCTION

Underwater creatures have always attracted both scientists and engineers for a long time due to their unique shape and swimming methods. Inspiration obtained from these underwater creatures helped mankind to determine the shape and propulsion mechanism of designed underwater vehicles. Actually, there is still one aquatic creature, namely the squid, whose underwater swimming performance both scientists and engineers have been investigating to understand. A squid unlike other fishes swims using her jet locomotion systems. Mainly, the mantle wall of a squid is used to store the water prior to move and when this water is squirted, a squid gains a significant amount of acceleration under water. Young et al., (1938) realized that circular and radial muscles of a squid plays an important role in jet locomotion system. They noted that circular and radial muscles belong inside and outside of the squid mantle wall and when the circular muscle applies tension on the squid's mantle wall, water flows out from the mantle cavity. Besides, radial muscle tension on the mantle cavity wall causes the mantle wall to become thinner and water is allowed to fill the mantle cavity. Later, Ward et al., (1972) studied the structure of the mantle wall and they documented that the mantle wall surface is entirely covered by tunic, which has large collagen fibers standing transversely to each other at specific angles. They also discovered that tunics are being connective tissue layers protecting both inner and outer surface of a mantle wall. In another study, Packard et al., (1974) claimed that jet locomotion cycle happens when the circular muscle is in tension and this is followed by a radial muscle activity to refill the mantle cavity. They also discovered that required jet force depends on timing of radial muscle activity prior to circular muscle contraction. Mommsen et al., (1981) analyzed the mantle wall and they showed the existence of two types of fibers, one of them is being glycolytic, 'rapid' fiber responsible for jetting while the other one is mitochondria-rich associated with normal swimming. Glycolytic fibers are located exclusively around radial muscles; therefore radial muscles are not used for normal swimming or breathing processes. They stated that the majority volume part of the squid mantle consists of circular muscles and these muscles are made from thick central layer of fast twitch layers Gosline et al., (1983) studied pressure variation and the change of a squid mantle wall diameter during a squid's swimming. They related hyper-inflated, jetting and refilling activities with the radial muscle, circular muscle and elastic recoil of the mantle wall, respectively. They also noted that squids fills their

mantle by seawater during water intake process and they eject the seawater with the help of the mantle wall to accelerate under the water by minimizing energy usage. In another study, Gosline and DeMont (1985) investigated a squid's mantle wall extensively to identify how a squid could produce such a large thrust. They realized that a squid inflates the mantle wall by keeping the mantle cavity at vacuum pressure so that water could be drawn into the mantle cavity prior to jet ejection. They documented the variation of pressure in the mantle cavity for both fast and slow swimming modes of squid. They also discovered that mantle wall thickness increases during jet ejection; therefore, the mantle wall structure could withstand the high pressure in the system. Later, Curtin et al., (2000) determined the relation between pressure and volume inside a squid mantle cavity. They also stated that the inner and outer sections of a squid mantle wall are covered by tunic layers. Their investigation concluded that when a squid mantle wall gets thicker during compression, the circular muscle contracts and the squid mantle wall muscle fibers produce a pressure yielding jet locomotion. Recently, Kurth et. al (2014) discussed variation of circumferential strain on the inner and outer surface of a squid's mantle wall during jet ejection. They also compared the mantle wall's inner surface with the outer surface in terms of shape change during escape jetting and they reported the variation of circumferential fibers for the mantle wall's hyper-inflation and contraction positions. More recently, Tabatabaei and Olcay (2015) studied the fluid flow characteristics of longfin inshore squids by using a numerical model generated from computed tomography images. They mainly focused on the drag force appearing on the squid body during her swimming and provided drag coefficient comparison between the squid and other aquatic creatures. Inspired by the incredible swimming performance of squids, a mantle wall of a squid was investigated for understanding the mantle wall's mechanical properties because this tissue plays a vitally important role in the fast swimming mode of a squid. Shape memory alloy based squid mantle actuation is done by using these parameters. Shape memory alloys are used as radial muscles and steel springs are as circular muscles.

Shape memory alloys are used many industrial applications such as; automotive, aerospace, orthodontia, robotics and so on. Shape memory alloys are commonly used because they can be controlled by temperature and pressure. Controlling by pressure and temperature makes shape memory alloys more usable areas. Shape memory alloys can remember their shape which makes them special alloy. Shape memory alloys go to original shape because of phase change crystallographic alloys to solid to solid phase. To observe phase transformation of

shape memory alloy, certain temperature or pressure were applied on shape memory alloy. Actuation temperature depends on shape memory alloy material and thickness. Shape memory alloys show two phases; austenite and martensite phases. Shape memory alloys show different properties during martensite or austenite. Lower than actuation temperature, shape memory alloys show martensite phase. Higher temperature, shape memory alloys show austenite phase. Martensite phase, material is monoclinic crystal structure. They can be deformed easily and they come back to original shape. They can be called as plastic. SMA alloys have special properties. When shape memory alloy is heated with electricity to actuation temperature, shape memory alloy starts to go back its memorized shape. They can memorize a certain shape by using heat from austenite to martensite. Phase change for SMA from austenite phase to martensite phase need high temperature. Shape memory alloys can get deform several times, but comes back to original shape by heating. Degeratu et al., (2008), made a research about shape memory alloy characteristic analysis, in that research shape memory alloy and conventional steel spring works against to obtain two way motion. Heating SMA spring pulls the steel spring and after cooling sma spring, steel spring pulls the SMA spring. Also, they analysis the heat analysis of SMA. For heat analysis, they built visual basic program software to get heat analysis result. They observed the sma thermal characteristic properties with respect to time. Brailovski et al., (1996), showed that, sma model characteristics depends on geometry, sma type and heat transfer condition. Geometry parameters are SMA's length and diameter. Heat transfer distribution on SMA is important and heat transfer efficiency plays big role to improve actuation of SMA. Khan et al., (2011), says, shape memory alloys shows nonlinear behavior unlike the other actuators. When load applied to shape memory alloys, SMA's strain and stress graph looks linear until a critical point.

In this thesis, there are two main topics. One is modelling a composite desing of squid mantle wall and another one is modelling of actuation based mechanical squid mantle cavity.

To create a composite model of squid mantle wall, compression, tension and shear test are needed. Test results are used to do a composite squid mantle wall same as real squid mantle wall tissue properties. Shape memory alloys, elastomer materials and steel springs are main materials to create composite squid mantle. Designing a composite design of squid mantle circular and radial muscle volume fractions are also needed. Circular muscles from squid mantle are used to create jet propulsion and radial muscles are used for slow swimming and water inhale to mantle.

Created actuation based on mechanical squid mantle cavity and observed smoke propulsion. Bellow was used as squid mantle and squeezed by steel spring to create smoke propulsion and observed smoke displacement and diffusion by laser. When laser light contacted the smoke, laser light showed the smoke location. From this idea, smoke displacement and smoke diffusion were observed. There were three different nozzles that were used, their dimensions were 2.5 mm, 5 mm and 10 mm. Three different spring diameters were used, 0.7 mm, 0.9 mm and 1 mm. Steel springs were used to squeeze bellow and shape memory alloys were used to pull steel springs. Mechanical squid propulsion's working principle was almost same as real squid's propulsion.



2. MATERIALS AND METHOD

Squids being from the family of cephalopod exhibit a unique swimming performance under water and are known to be the fastest swimmers in aquatic invertebrates by using their jet propulsion system. They use an unsteady jet propulsion for fast swimming mode while they initiate the fin movement for slow swimming mode. In fast swimming mode, a squid inflates her mantle wall causing vacuum pressure in the mantle cavity. This actually yields water around the squid's head to be inhaled through the openings near her eyes. Prior to move, a squid applies contraction to her mantle wall and pressurizes the water in the mantle cavity. Then, she ejects the water through the nozzle in the form of jet propulsion while she accelerates towards the opposite direction of the jet as given in Figure 2.1. This virtually gives the squid a priceless opportunity to escape from her enemy or to catch her prey.

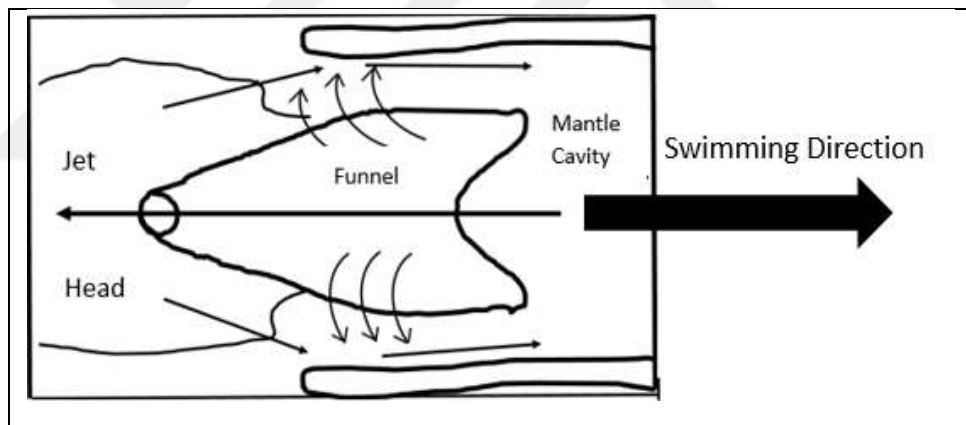


Figure 2.1. Jet cycle schema

Figure 2.1 gives details about squid locomotion system and these details give opinions about designing squid mantle. Squid's mantle wall has two types of muscles. These are circular and radial muscles. Circular muscles squeeze mantle wall to create water propulsion, during propulsion radial muscles do not involve. Radial muscles start to activate after propulsion to suck water to inside mantle cavity. This gives the idea to design mechanical squid. Steel springs and radial muscles are chosen as circular and radial muscles respectively. Squid squeezes mantle cavity circular direction, but it is hard to create a circular pressure, mechanical squid squeeze its mantle in linear direction as seen in Figure 2.2.

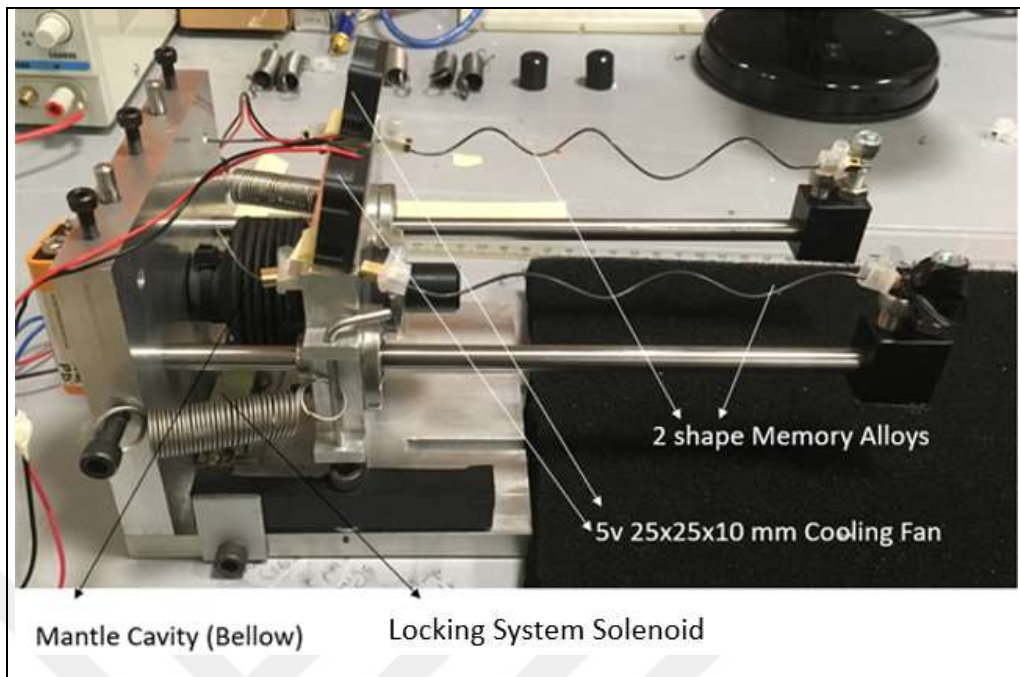


Figure 2.2. Complete Model of Mechanical Squid Mantle Testing Device

Inspired by squid propulsion system, bellow as squid mantle, circular muscles as steel springs and shape memory alloy as radial muscles are used. Figure 2.2 shows used testing devices and parts are aluminum 8000m series, bellow, shape memory alloys, steel springs, pulley, power supply, cooling fan and locking system solenoid. Aluminums are used to hold the bellow, high speed cameras are for recording the smoke propulsion. To observe smoke, a laser is used. Instron machine is used to find spring constant of bellow as shown in Figure 5.7. Power supplies are to heat the shape memory alloys. The laser is placed in front of the nozzle to observe smoke location. The steel springs stretch the aluminum profile and bellow is compressed by them. The smoke inside of the bellow is flow out and high speed camera will record. The power supply gives voltage to heat the shape memory alloys to make the experimental setup to original shape. After that, solenoid locks the system and cooling fans cool the shape memory alloys. Cooled shape memory alloy becomes softer than heated. After cooling process to shape memory alloy, applied voltage to solenoid to unlock the system. When system is unlocked, steel springs are activated to squeeze the system.

3. SQUID MANTLE WALL MECHANICAL PROPERTIES

To observe and understand the squid water locomotion system, squids anatomic structures and squid mantle tissue properties must be observed. Tissue properties are analyzed from tensile test, shear test and compression test. Tensile stress, shear stress and compressive stress values are found to design almost same as real squid properties value to create composite squid mantle wall.

3.1. TENSILE TEST EXPERIMENT

Tensile test basic idea, there is a placed material and clamped with two hooks. Material dimensions are known cross section, thickness and length. During load applied to material, tension is applied on it and recorded to measuring dimension change. Material strength is found by tensile test. In order to understand mechanical properties of squid mantle wall, squid mantle wall's tissue specimen was placed to Instron machine (Instron 3382J, Norwood, MA, USA) to tensile testing. Seven different longfin squids weighing between 100 gr and 200 gr were used to find mechanical properties of squid mantle wall. The lengths, weights, nozzle diameters and mantle lengths were measured and given in Table 3.1. The mantle walls of squids are disemboweled and then cut into pieces to be tested in tension, compression and shear testings. The disemboweled pieces were obtained in a ring shape so that they could be placed into experimental setups. The specimen, which has circular ring shape, was placed to Instron machine's upper hook as shown Figure 3.1. The specimen lower side was fixed to Instron machine. Load is recorded via load cell and data recorded with displacement respect to: 1.0, 7.5 and 15 mm/min. The dimensions required in the calculation of the nominal cross-section area and also the initial gauge length of the specimen were measured and recorded before the test started. These measurements were repeated for every specimen.

Table 3.1. Measurements of the squid's geometrical dimensions

Squid CT Scan	Length (in cm)	Mass (gram)	D_{nozzle}	D_{mantle}	L_{mantle}
1	40.5	158	0.95	4.1	16.5
2	29	74	0.7	3.3	12
3	34	114	0.9	4.5	15
4	32.5	98	0.9	3.9	14
5	37	164	0.8	4.4	14.5
6	43.5	194	1	4.9	17
7	42	190	0.9	4.9	17

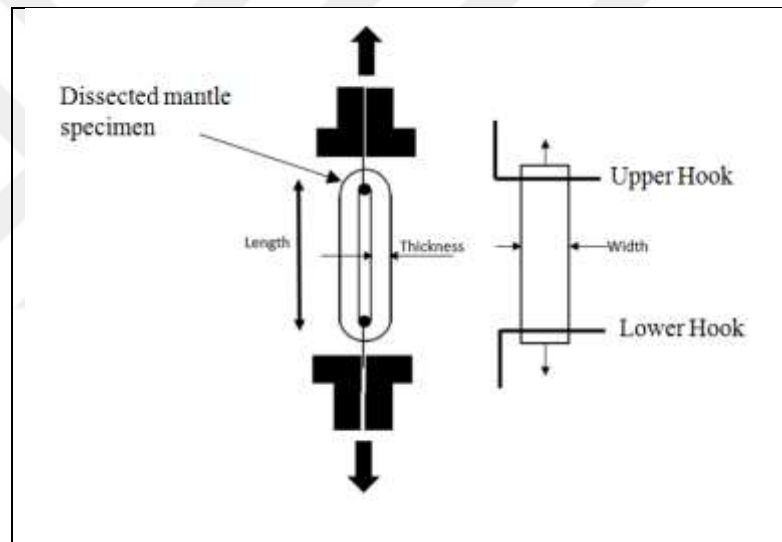


Figure 3.1. Front and side view of circular specimen with tensile test

The mantle wall consists of several muscle structures. Gosline and DeMont (1985) described the fibers forming the mantle wall tissue as circular, radial and longitudinal muscles as depicted in Figure 3.2. When the shape of a mantle wall is examined during water inhales and exhales, it is noted that the circular muscles were primarily responsible for the contraction and expansion of the mantle wall. However, the radial muscles are associated with the variety of the mantle wall's thickness and the longitudinal muscles nearly remained unchanged across the mantle length. Since the present study focuses on circular muscles of a mantle wall, the mechanical properties such as modulus of elasticity, stress-strain behavior and the Poisson's ratio of the circular muscle are determined. Tensile testing provided

information about the material's property including yield point, tensile strength, and elongation. Stress-Strain behavior of each specimen are also obtained.

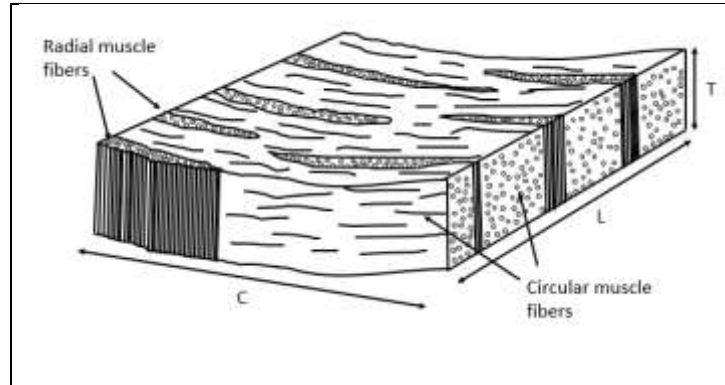


Figure 3.2. Diagram of a piece cut from the squid mantle wall

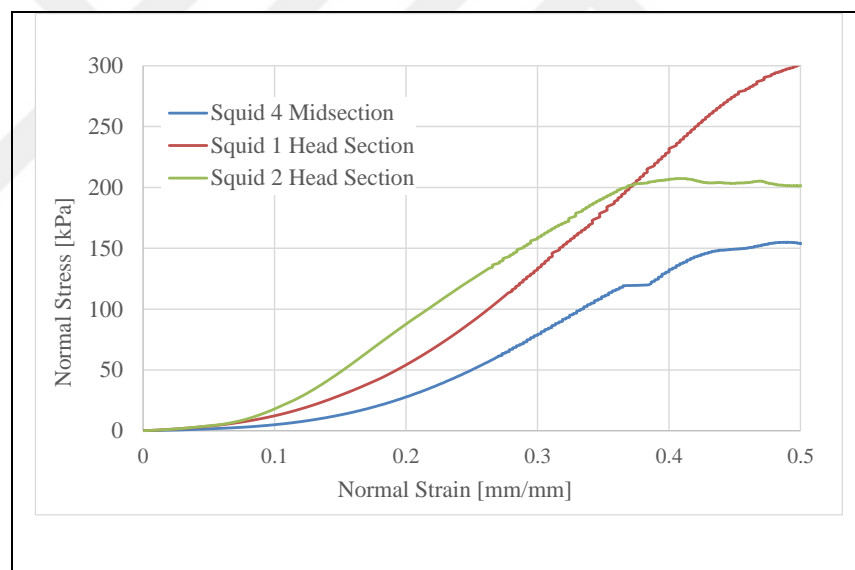


Figure 3.3. Stress/strain curves resulting from a single loading cycle of three different squid mantle tissue blocks

Figure 3.2. shows schematic view of the radial and the circular muscle fibers. Here C, T and L show the circumferential, thickness and the longitudinal directions of the cut, respectively. Circular muscles play important role to squid locomotion system. Squid squeezes the circular muscles of mantle wall to let the water outside. On the contrary, radial muscles pull the circular muscles to inhale water inside the mantle cavity.

Stress and strain were calculated and plotted for each trial as shown in Figure 3.3. During the first 0.1 mm/min of tensional strain (10% strain), little resistance was observed; thereafter, the stress increased gradually. Here, force was expressed as stress (force divided by the area, $T \times L$, see Fig. 3.2) and strain was the ratio of change in length C to the initial value of C . The initial value of C was the length at which tension first produced measurable force by the load cell. The elastic modulus was calculated using the linear regression to this linear part of the curve; between the strains 0.15 and 0.32 mm/min. Three cases were tested with similar tissues taken from the approximately same sized squids. A strain rate of 7.5 was applied in one case and Young's modulus was calculated as 536.1 kPa as tabulated in Table 3.2. The strain rate was increased to 15 mm/min for the other two cases and Young's modulus were calculated as 706.4 kPa and 877.4 kPa respectively. Circular muscles fibers could not resist when the normal strain level between 0.4 and 0.6 mm/mm. At strain levels higher than 0.4 mm/mm the circular muscle fibers started to fail under tension. Mantle wall is a viscoelastic material because of that reason different strain rates (1.0, 7.5 and 15 mm/min) were used to find the best quasi-static condition and 1.0 mm/min selected to find the elastic properties of the tissue.

Table 3.2. Small sized-squid midsection and heading tensile test young's modulus results

Small-Size Squid	Tensile Test Speed	Young's Modulus
Squid 1 Head Section	15 mm/min	877.4 kPa
Squid 2 Head Section	15 mm/min	706.4 kPa
Squid 4 Mid Section	7.5 mm/min	536.1 kPa

3.2. SHEAR TEST EXPERIMENT

During tensile test, tensile force applied to squid mantle wall tissue on circular direction. To understand the how much tensile force squid needs when squid takes water inside to its' mantle wall.

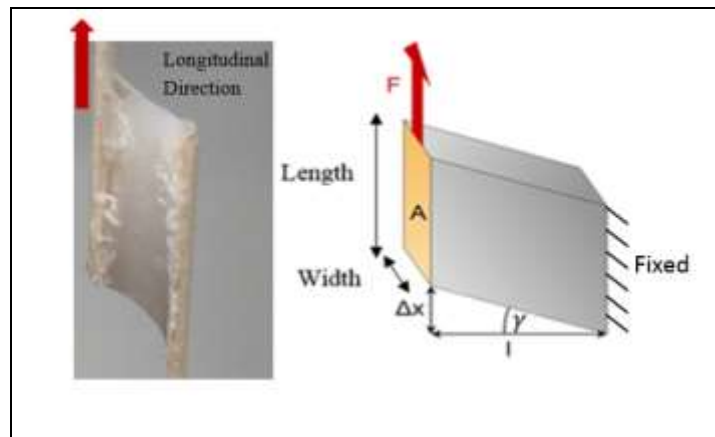


Figure 3.4. Front view of shear testing specimen

A small piece cut from the mantle wall was subjected to a shear force as shown in Figure 3.4 to determine the characteristics of the mantle wall tissue. Here, shear force was applied to the outer and inner surfaces of the cut specimen in a circular direction. It was noted that the mantle wall tissue was prepared as a rectangle block specimen and these specimens were used in shear stress tests because the specimen needs to have a certain thickness to be able to precisely observe shear strain. Because of this, the squids with the thickest mantle walls were selected for the shear stress test measurements. In the shear stress test apparatus, two rectangle block specimens were taken from the thickest portion of the mantle wall. Squid mantle wall tissue's left section had a width of 15 mm, a length of 20 mm and a 5.5 mm of thickness and the top section had a width of 15 mm, a length of 18 mm and a 4.3 mm of thickness. Shear test is done by using Instron device. Prior to the test, dimensions for each specimen were recorded as shown Table 3.2. Force versus displacement datum were recorded and then used in the calculation of the engineering shear stress and shear strain.

Table 3.3. Thickness measurement and area calculation of top section and left section

Medium-Sized Squid Section 5	Initial Thickness (mm)	Area (mm ²)
Top section	5.5	300
Left section	4.3	270

A squid applies tension or compression on her mantle wall during jet locomotion. A mantle wall endures tensile, compressive and shear strength under these loads. In this part of the

work, the shear strength of a mantle wall was identified for the specimens tested. Specifically, shear test experiments were performed using an Instron tensile test machine. Squid mantle wall tissue tore around 7 kPa shear stress value, see Figure 3.5. The modulus of rigidity was calculated by using linear regression to the linear part of the shear stress strain response of the specimen and found to be approximately 11.4 kPa. The sudden decrease that was observed in the beginning of the stress-strain response of the curve (between 0.6 – 0.7 shear strain) is happening due to the delamination of the tunic tissue of the mantle wall.

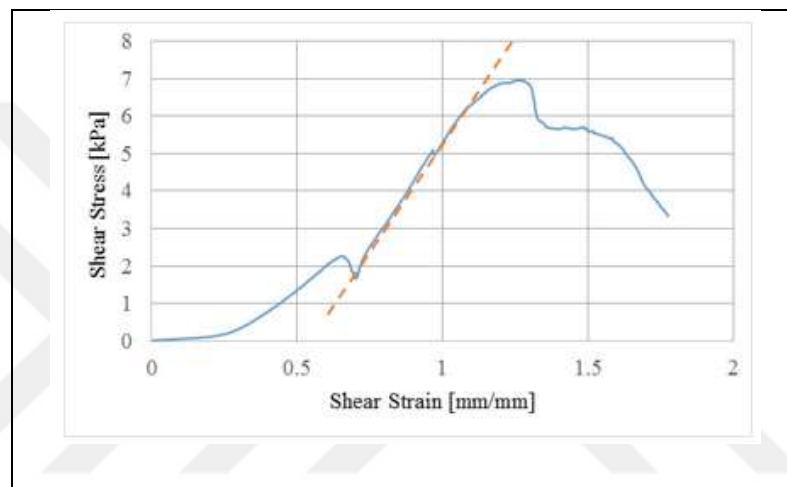


Figure 3.5. Shear stress strain behavior of the mantle wall tissue

3.3. COMPRESSION TEST EXPERIMENT

In tensile test experiments, the deformation of the mantle wall was similar to that produced by elongation of the circular muscle fibers. Also, to examine what happens when the radial muscle fibers shorten, further experiments were done where mantle wall tissue were prepared as disc shape specimens compressed in the transverse direction as shown Figure 3.6. During jetting, squid compresses its mantle wall to flow water outside the mantle. under tension during water inhale and it becomes under compression during water exhale, a.k.a. water ejection. It is known that when any material is compressed in one direction, it usually tends to expand in the other two directions perpendicular to the direction of compression due to Poisson's effect. Therefore, in this part of the study, compression test measurements were performed on a mantle wall to understand the mechanical behavior of the tissue during jet propulsion. Poisson's ratio (ν) represents the degree to which a material expands

transversely as it is strained (compressed) axially. Poisson's ratio, also called Poisson's coefficient, is limited between values of 0 and 0.5. While materials with $\nu = 0.5$ are known to be incompressible, materials with $\nu = 0$ are referred to be completely compressible. Disc shape squid tissue was tested with Instron machine with constrained and unconstrained situations to find out the Young's modulus values. After that, Poisson ratio value is found by taking ratios of constrained and unconstrained Young modulus values.

$$\frac{E_0}{E_b} = 1 - \frac{2\nu^2}{1 - \nu} \quad (3.1)$$

Where E_0 represents unconstrained Young's modulus and E_b represents constrained Young's modulus.

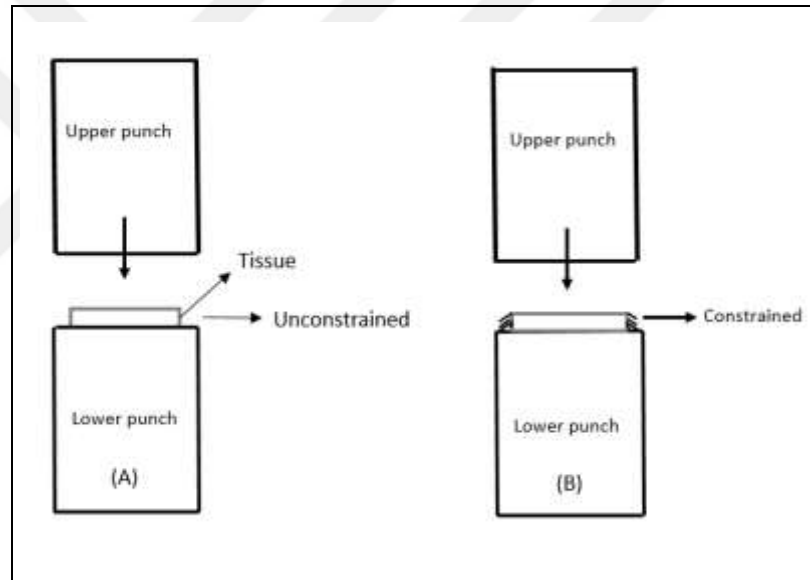


Figure 3.6. Unconstrained and constrained compression test

In this compression test experiment, incompressible materials are compressed axially, their volume must remain constant and they expand laterally but when completely compressible materials are compressed axially, they do not expand laterally. Used tissues in Figure 3.4. just like the ones used in shear testing, were cut into a disc shape specimen and used for compression test. The disc shaped tissue with a 22 mm diameter and a 5.7 mm thickness was placed between Instron's compression punches and then a compressive displacement with 1 mm/min strain rate was applied as shown in Figure 3.6. In elasticity measurements, it was important that samples remained unconfined or unconstrained laterally as they were

compressed axially; therefore, two cases were measured as unconstrained and constrained compression cases. The elastic response of these two compression tests were used to calculate Poisson's ratio for the mantle wall tissue.

Results were obtained from two testing cases of the mantle wall tissue; Figure 3.6 (A) shows the constrained compression test and Figure 3.6 (B) gives the unconstrained compression case findings. In both results, during the first 0.1 mm/min of compressive strain (10 % strain) there was little resistance similar to the observation made in the tension test; thereafter, the value of stress increased. In the steeper part of the curves, stress was almost a linear function of strain implying that the stiffness was constant. The elastic modulus was calculated using the linear regression to the linear part of the curve. Stress-strain curve resulting from constrained test and unconstrained Young's modulus was found to be 620.3 kPa in Figure 3.7 (a). Compressive stress-strain curve resulting from unconstrained compression test and Young's modulus was found 400.1 kPa in Figure 3.7 (b).

In this part, specimens were compressed to reach Poisson's ratio value. Poisson's ratio was calculated using below equation.

$$\frac{E_0}{E_b} = 1 - [2\nu^2/(1 - \nu)] \quad (3.2)$$

E_0 represents calculated unconstrained Young's modulus, E_b represents constrained Young's modulus. Poisson's ratio is found 0.34 for the mantle wall tissue.

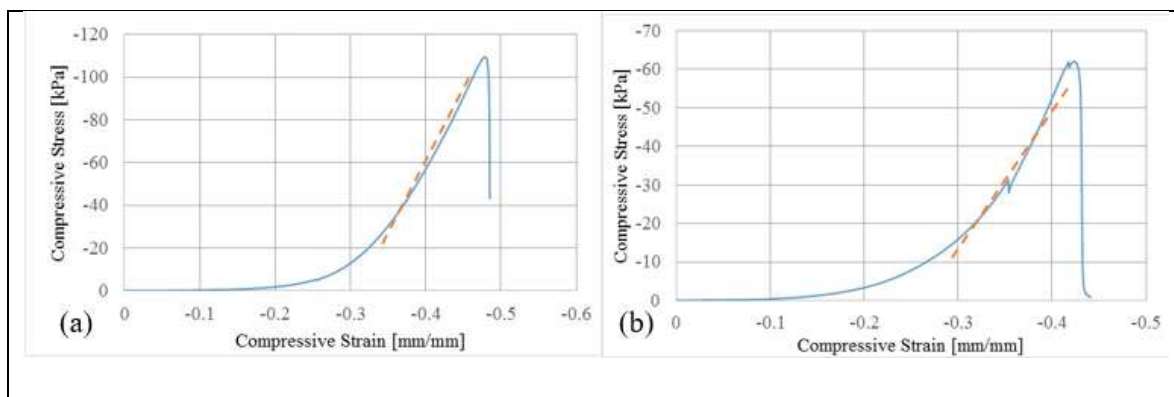


Figure 3.7. Compression test results showing the stress strain relationship for constrained compression test and unconstrained compression test

In tensile test experiment, the deformation of the mantle wall was similar to that produced by elongation of the circular muscle fibers. Also, to examine also what happens when the radial muscle fiber shorten, further experiments were done in which mantle wall tissues were prepared as disc shape specimens compressed in the transverse direction as shown in Figure 3.6. Results obtained from two testing cases of the mantle wall tissue; Figure 3.7(a) shows the constrained compression test while Figure 3.7(b) gives the unconstrained compression case findings.

3.4. SQUID MANTLE WALL WORKING PRINCIPLE

Squids are cephalopod invertebrates. It has a symmetrical body structure. Eyes are in the middle of its body. They have eight arms surrounding the mouth and two tentacles that are long in the obvious amount. A large part of the squid's body forms a thick muscle blanket called the mantle, which protects the internal organs and allows the squid to move in the water. Below the body there are two gills, breeding area and secretion in the area close to the mantle. Two triangle shaped fins attached to the mantle and fins float in the water. But these fins do not play role to squid move inside water. Squids squeeze their mantle to water propulsion after that, returns the water backward to mantle cavity by spraying water at high speed. Thanks to mantle cavity shape like, funnel makes a jet effect, so squid can speed up. Squid can swim short distance in a short time by using jet. Squid body covered with color pigment makes easy to run from their enemy and also helps squid to become a hunter. When in danger, the squid's ink is sufficient to camouflage and to escape quickly. Human's tanned pigment is the same as the squid's melanin pigment. For squid habitat, they have to live in a specific place, that place has a certain temperature and salt rate, so that is located in the waters of Turkey. Squids typically produce powerful jets by impulsively ejecting the water initially in their mantle cavity. Therefore, a mantle cavity of a squid plays a key role when a mantle wall tissue applies a significant pressure to the water inside the mantle cavity prior to accelerate.

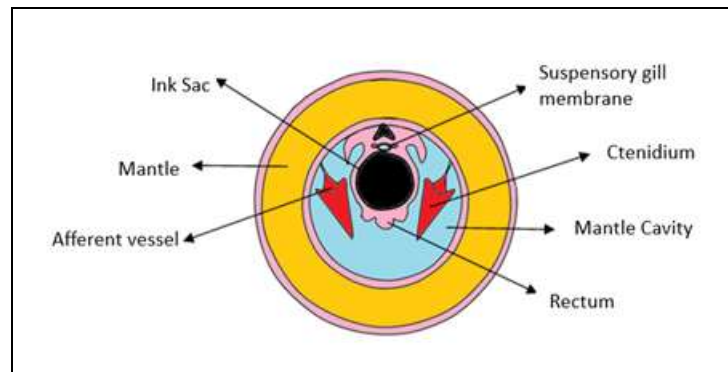


Figure 3.8. Cross section of squid mantle cavity

Figure 3.8. shows anatomic structure of squid mantle cavity. There are two types of mantle of squids. Mantle cavity is used for jet. Mantle is used for digest their food. Ink sac is throwing ink to run away from their hunters. Rectum is for discharge.

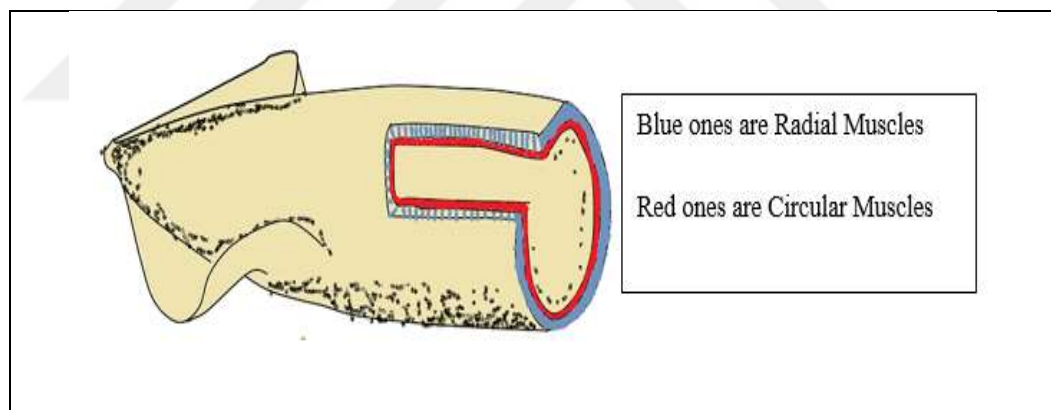


Figure 3.9. Squid mantle wall circular and radial muscles relation

Circular muscles are responsible from create the pressure that is necessary to create the jet propulsion. Figure 3.9 shows the location of circular and radial muscles in squid mantle wall. They are connected to each other. This Figure plays important role to create a composite squid mantle wall design. Radial muscles are between squid skin and circular muscles and there is a tunic to make radial muscles move comfortably.

4. SQUID MANTLE WALL COMPOSITE DESIGN

Squid mantle wall's composite model is designed based on unidirectional short fiber composite. After tension test results, composite Young's modulus value is found by using this formula 4.1. E_c is used as tension test Young's modulus value.

$$E_c = E_f V_f + (1 - V_f) E_m \quad (4.1)$$

Table 4.1. Mechanical properties of nitinol

Mechanical Properties of Nitinol	Values
Approximate Elastic Modulus (hi-temp)	75 GPa
Approximate Elastic Modulus (low-temp)	28 GPa
Approximate Poisson's Ratio	0.3
Elongation to Fracture	15.5 %
Actuation Energy Conversion Efficiency	5 %
Density	6.45 gr/cc

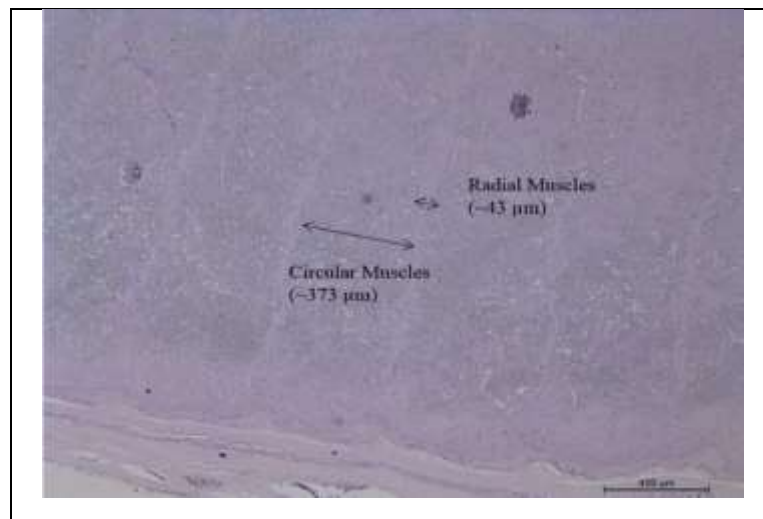


Figure 4.1. Micrographs of squid mantle shows circular and radial muscle arrangement

The mantle wall of a squid is mainly made of circular and radial muscles. Since squids heavily depend on circular muscles for their jet propulsion, circular muscles of a squid

should occupy a large part of the mantle wall tissue. Circular muscle distribution is found micrographs of squid mantle Figure 4.1, which is 8.6 times greater than radial muscle. Circular muscle occupies more place than radial muscle. Therefore circular muscle was as fiber, radial and squid mantle wall were as matrix. Fibers are used as active fiber. Because of water taking in, out and steady position. Fibers must change their length.

Table 4.2. Squid mantle wall tissue

Squid Mantle Wall Tissue	Values
Approximate Elastic Modulus	500-900 kPa
Approximate Poisson's Ratio	0.34
Volume Fraction of Matrix	14%
Volume Fraction of Fiber	86%
Approximate of Modulus of Rigidity	170-300 kPa

Circular muscles are responsible for squid mantle to contract and create the pressure that is necessary to form the jet repulsion. Because of this reason for the squid mantle, the circular muscles are chosen as fiber phase of the composite modeling while the radial muscles together with the remaining connecting tissue are treated as the matrix phase. Shape memory alloy (SMA) material is also integrated into the matrix phase to imitate the hyper-inflation stage. Figure 4.3. shows the front and side view of the model cross-section, the steel springs embedded in the elastomer will imitate the contraction stage and the SMA springs connected to outer fixed ring will be activated in the hyper-inflation stage in order to increase the mantle cavity volume. Radial muscles are between mantle cavity and squid body. Therefore radial muscles can not resist water flow. SMA of strain rate is less than approximately % 15. Therefore, steel spring is used for SMA. Radial SMA are used as bias spring. During jetting process, mantle cavity looks like circular shape to create jet. Therefore, outside shape is fixed and circular.

During jetting, squid mantle wall stretch itself very fast. Steel spring was chosen because it squeezes fast. After locomotion process, mantle wall must get back to the original shape for hyper-inflated. Therefore shape memory alloys pull the mantle wall to get its original shape. When mantle wall gets the original shape, mechanism holds the mantle wall stable. Mechanism triggers the steel spring to jet locomotion. Nitinol elastic modulus values in hi-temp 75 gPa and low-temp 28 gPa. Steel's (ASTM-A36) young modulus value 200 gPa.

Volume fraction of fiber was 0.37 and matrix was 0.63. Using rule of mixture method composite young modulus found 74.03 gPa.

Squid's mantle cavity thickness and diameter changes depend on slow swimming and jet escape as shown below inside Table 4.3.

Table 4.3. Squid mantle cavity change by slow swimming and jet escape

Squid's Mantle Cavity	Slow Swimming	Jet Escape
Diameter (m)	0.021-0.019	0.023-0.014
Thickness (m)	3.5×10^{-3} - 3.7×10^{-3}	3.5×10^{-3} - 5×10^{-3}

During squid mantle cavity diameter and thickness changing happens time dependent is 0.45 second.

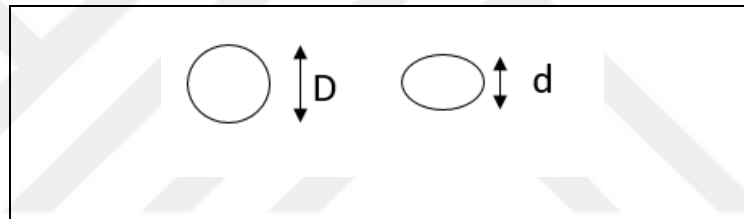


Figure 4.2. Squid nozzle diameter change

Squid mantle wall Figure 4.2 shows the mantle nozzle shape during water taking into mantle wall and taking out to sea. When mantle wall is contracted, radial muscles get larger and the circular muscles contract the mantle therefore water goes outside from mantle cavity. To let water inside the mantle cavity, radial muscles inside mantle wall get smaller and pull circular muscles. After that, water goes inside mantle cavity. Squid's mantle cavity is squeezed by circular muscles to create jet propulsion.

Diameter change in slow swimming contracted mantle over uncontracted mantle is 1.206 and diameter change in jet escape ratio is 3.25. Mantle volume change ratio is found 2.5.

Table 4.4. Elastomer and steel spring properties

Elastomer Young Modulus	10 MPa
Steel Spring Young Modulus	200 GPa
Steel Spring Modulus of Rigidity	75.8 GPa
Free length of Spring	30 mm
Spring Inner Diameter	5 mm
Spring Outer Diameter	7 mm
Spring Diameter	1 mm
Mean Diameter	8 mm
Steel Spring Constant	4.39 N/mm
Total Wire Length	14.7 mm
Volume of One Single Steel Spring	115.45 mm ³
Area of Composite Squid Mantle Wall	1260 mm ²
Total Volume of Composite Squid Mantle Wall	88200 mm ³
Number of Steel Spring	30
Steel Spring over Total Volume	39.26%

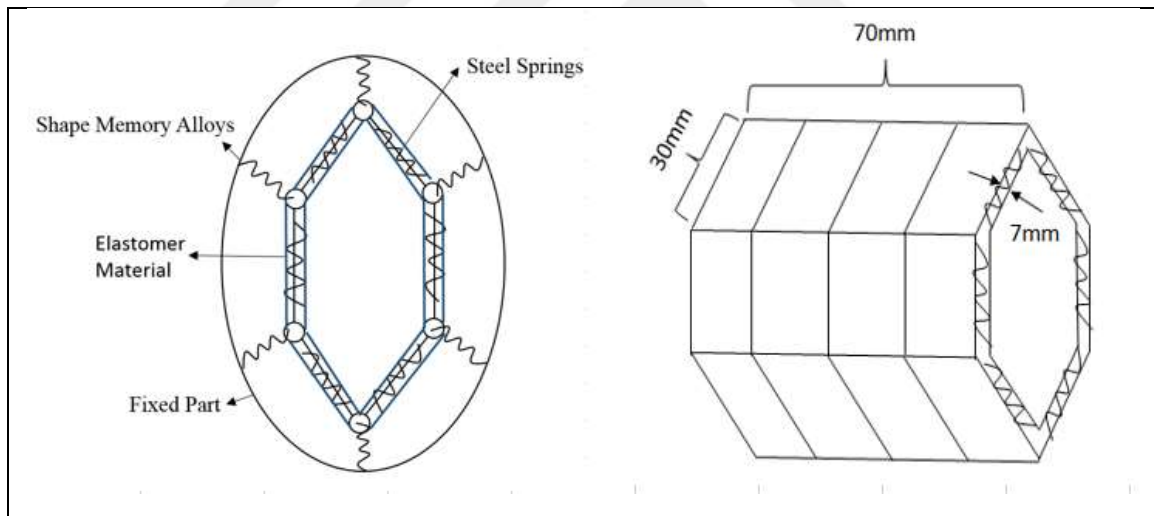


Figure 4.3. Squid mantle cavity composite structure front and side view

Figure 4.3 shows composite design of squid mantle cavity, squid mantle is designed as hexagonal shape. Mantle acts like plastic, during water inhale and exhale. Therefore, elastomer material is used as mantle wall. Inside of elastomer material, there are steel springs. These springs are used as circular muscles, to create water propulsion. Elastomer materials are connected with each other. Shape memory alloys are used as radial muscles to water inhale. SMA pull circular muscles to take water inside mantle. There is a fixed part,

which is used as adventitia. To protect mantle from outside. Each steel springs length is 30 mm and mantle side length 70 mm. Table 4.1 and Table 4.4 shows the elastomer, steel spring material and shape memory alloy properties. Table 4.2 and Table 4.3 show the squid mantle wall material properties from tensile, shear and compression test results and squid nozzle dimension during slow swimming and jet. Steel spring, elastomer materials and shape memory alloys volume fractions are found. Steel spring, shape memor alloy and elastomer materials' mechanical properties are found and then used rule of mixture to find composite design material properties. With using these parameters composite squid mantle cavity design is made.

Table 4.4 shows the total mantle cavity volume, which is needed to calculate volume change of composite squid mantle during jet. It is known that, squid mantle cavity volume change ratio is 2.5. During jet, squid mantle cavity volume is found from total volume and volume change ratio, squid mantle cavity volume is found 55920 mm³ in jet. Volumetric flow rate over nozzle area is given jet speed, which is 33 m/s. Jet speed and water mass are known and used in kinematic energy formula and found 16.99 joule. Spring diameter distance change is also found from mantle volume change, is 18 mm. Spring static energy is found 21.33 joule. Propulsion efficiency is found 0.79.

5. SHAPE MEMORY BASED SQUID DESIGN

Shape memory alloys have unique properties which make them special alloys. They can change their shape when pressure or temperature are applied. Shape memory alloys are used in industrial applications. Shape memory alloys actuation temperature depends on their thickness and material properties. Squids are known to be the fastest swimmers in aquatic invertebrates because of their unique swimming performance under water. They have self-propelled system in their mantle wall. Shape memory alloy is used in mechanical squid to make mechanical squid self-propelled pulsed-jet.

5.1. SHAPE MEMORY ALLOY HEATING

Shape memory alloys are used in many industrial applications such as; automotive, aerospace, orthodontia, robotics and so. Shape memory alloys are commonly used because they can be controlled by temperature and pressure. Controlling by pressure and temperature makes shape memory alloys more usable. Shape memory alloys can remember their shape which makes them remarkable alloy. Shape memory alloys go to the original shape because of phase change crystallographic alloys to solid to solid phase as shown Figure 5.1. To be able to see the phase transformation of SMA, applied certain temperature or pressure to shape memory alloy. Actuation temperature depends on shape memory alloy material and thickness. Shape memory alloys show two phases; austenite and martensite phases. Shape memory alloy shows different properties during martensite or austenite. Lower than actuation temperature, shape memory alloys show martensite phase. In higher temperature, shape memory alloys show austenite phase.

Martensite phase, material is monoclinic crystal structure. They can be deformed easily. They become plastic. SMA alloys have special properties. When applied electricity, stress or heat on SMA, SMA starts to actuate. SMA can be memorized to a certain shape by using heat from martensite to austenite phase. Heat or applied stress, determine what phase the SMA will be; on high temperature SMA is austenite phase, martensite phase at low temperature. Stress and temperature gets higher SMA gets austenite phase. Applied stress and temperature gets lower, SMA phase goes to austenite to martensite. Same as super-elastic material has martensite phase just like SMA. Changing shape of super-elastic material

at room temperature, super-elastic goes back to original shape at room temperature. Means that austenite to martensite at room temperature unlike SMA. In this thesis, SMA is used as spring shape, which has 4 number of turns. SMA is wrapped around a metal stick. It is heated inside oven to memorized as a coil shape. Oven heating degree is set to 250°C and waited almost 45 minutes. After heating process, SMA is put inside a cold water bath and waited 30 minutes to get martensite phase.

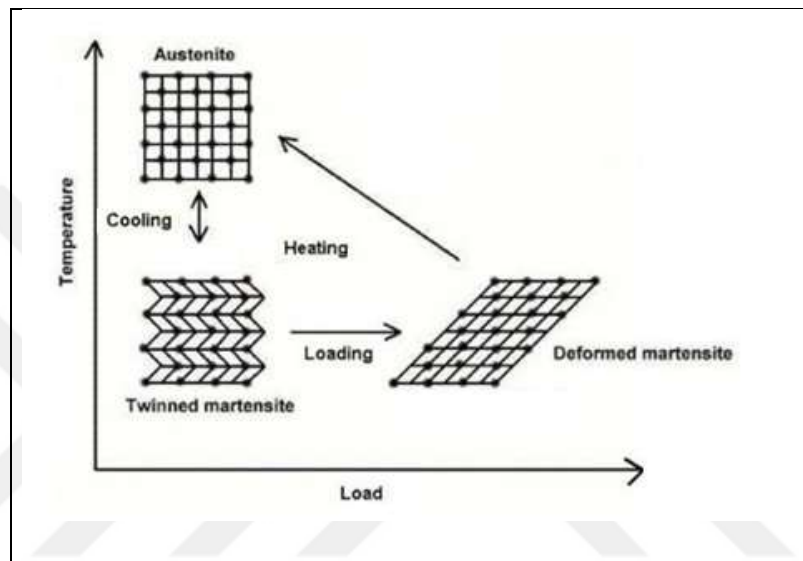


Figure 5.1. Diagram of shape memory alloy's microscopic structure

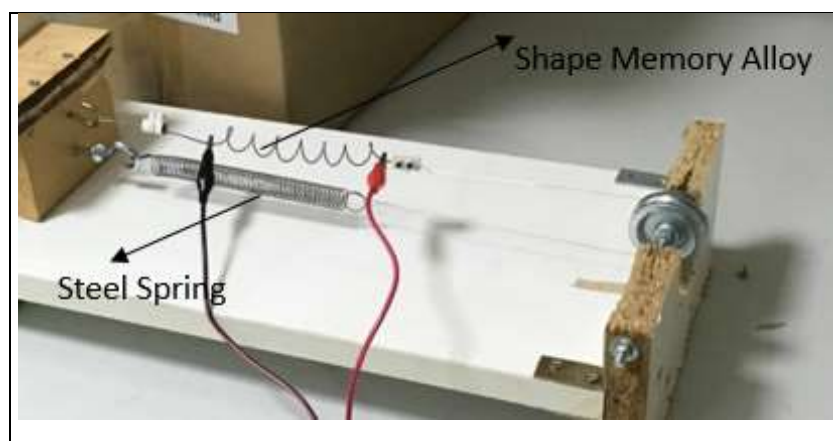


Figure 5.2. Shape memory alloy and steel spring

Figure 5.2 shows steel spring and shape memory alloy to observe them, they can pull each other. There is a pulley design one side hanged with steel spring and other is shape memory alloy and there is power supply to heat shape memory alloy to pull steel spring. As squid mantle cavity, used a bellow. Bellow's longitudinal length is 77 mm from Figure 5.6. In this experiment needs that, shape memory alloy pull to steel spring 35 mm. When squid creates water propulsion, they squeeze their mantle almost half of it. Therefore shape memory alloy pulling distance is 35 mm.

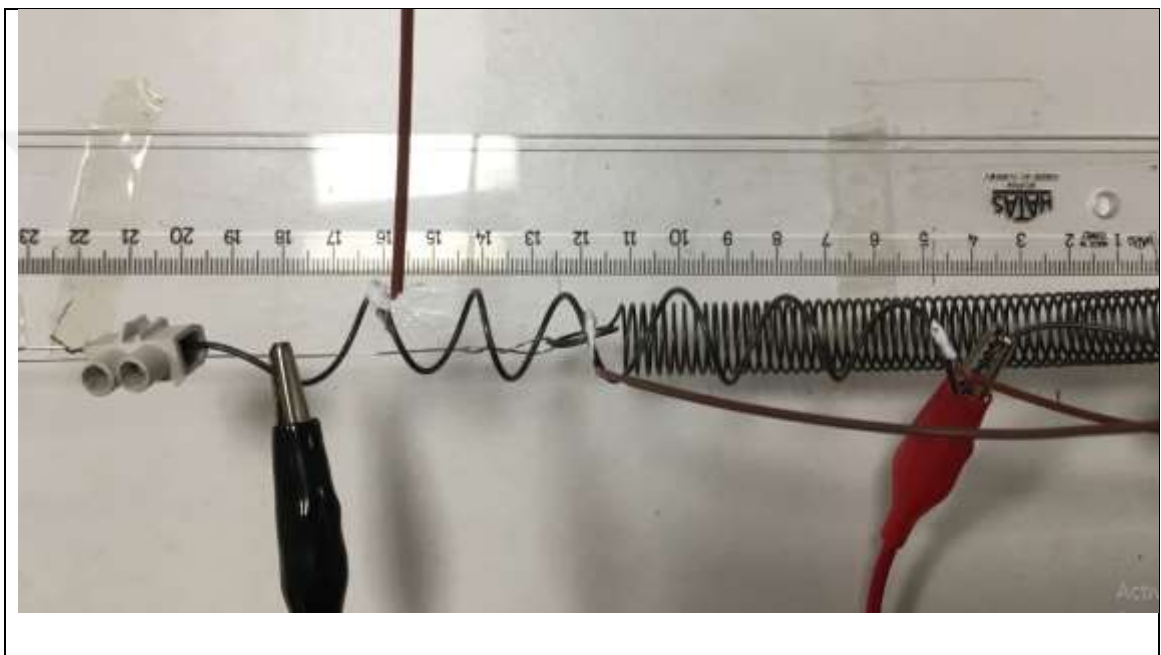


Figure 5.3. Shape memory alloy and steel spring movement length

In this master thesis, two way spring is used. This project takes inspiration from squid water jet. Squid mantle cavity has two types of muscles. These are circular and radial muscles. Circular muscles do the main job for jetting. Therefore steel springs are used like circular muscles to create fast propulsion. Radial muscles are shape memory alloys. In order to use shape memory alloy and steel spring together in Figure 5.2 test setup is done. Like taking water inside mantle cavity and throw out to outside. Steel springs and shape memory alloy must work together. They must have power to pull each other and need to test them. For example, during jet steel springs squeezed the bellow (mantle) and shape memory alloy pulls back the bellow to original position. Figure 5.3 shows that, heated SMA can pull the steel

spring and after that, steel spring can pull the SMA, during cooled sma. DC voltage reading shows that, 5.3 amper and 1.2 voltage is enough to pull the steel spring.

After testing, the SMA and steel spring works together. Found the SMA's martensite and austenite start and finish temperature and applied voltage by using thermocouples and DC power supply.

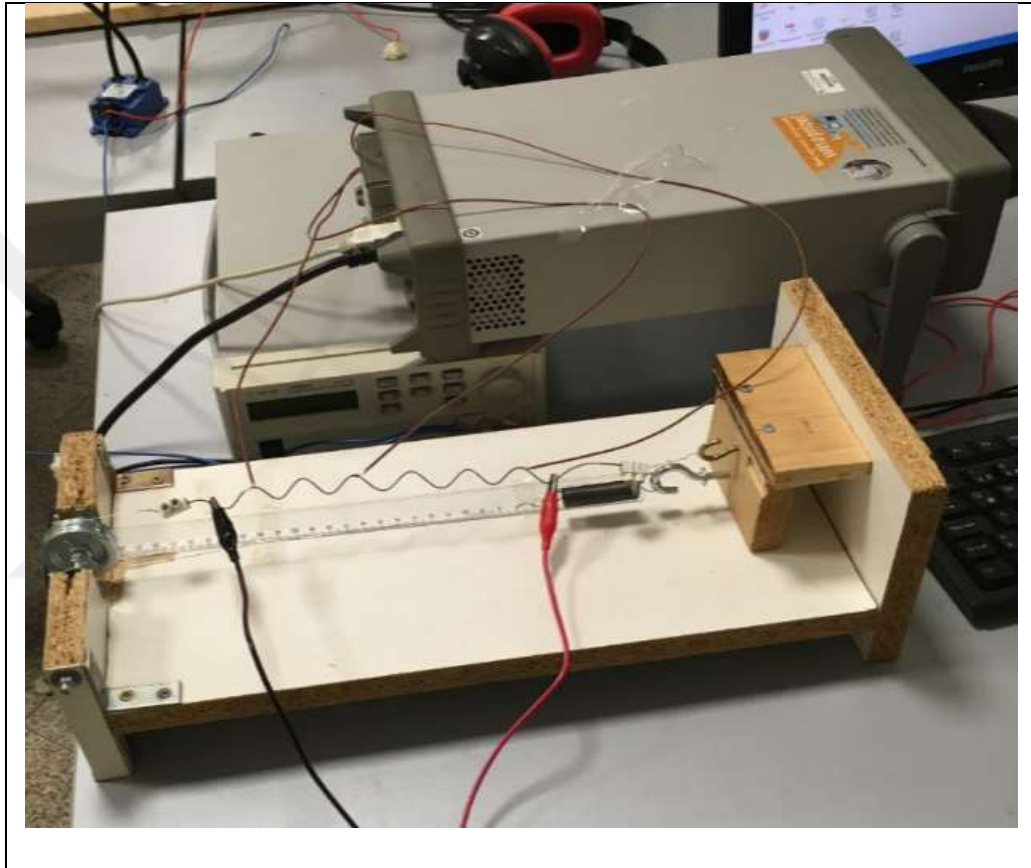


Figure 5.4. Shape memory alloy applied voltage and measuring actuation temperature with thermocouple

To create phase change for SMA from austenite phase to martensite phase need high temperature. Shape memory alloys are commonly used because they can be controlled by temperature and pressure. For temperature controlled shape memory alloy actuator, important argument is determination of actuation temperature. Differential scanning calorimeter (DSC) is used to determine the phase transformation temperature of shape memory alloy. DSC is not used the spring type of shape memory alloy, DSC is used when it is powder form.

Choon et. al (2007) was decided to find shape memory alloy's martensite and austenite start and finish values not using DSC. Because in order to use DSC, need to get the SMA powder form. They used a universal testing machine to find martensite and austenite start and finish values. Heating up and after cooling down the SMA by using DC power supply and during heating and cooling they recorded the SMA alloys length with different force applied on SMA. After that, they found the SMA martensite and austenite start and finish values without using DSC. Same as Choon et., al (2007), in Figure 5.4. applied DC voltage to shape memory alloy and also thermocouples attached to it. When applied voltage to SMA thermocouples show the temperature increases and shows the martensite and austenite start and finish temperatures and voltages. Figure 5.4 shows to how to record data and the used bench link data logger computer software to understand the heat distribution in time.

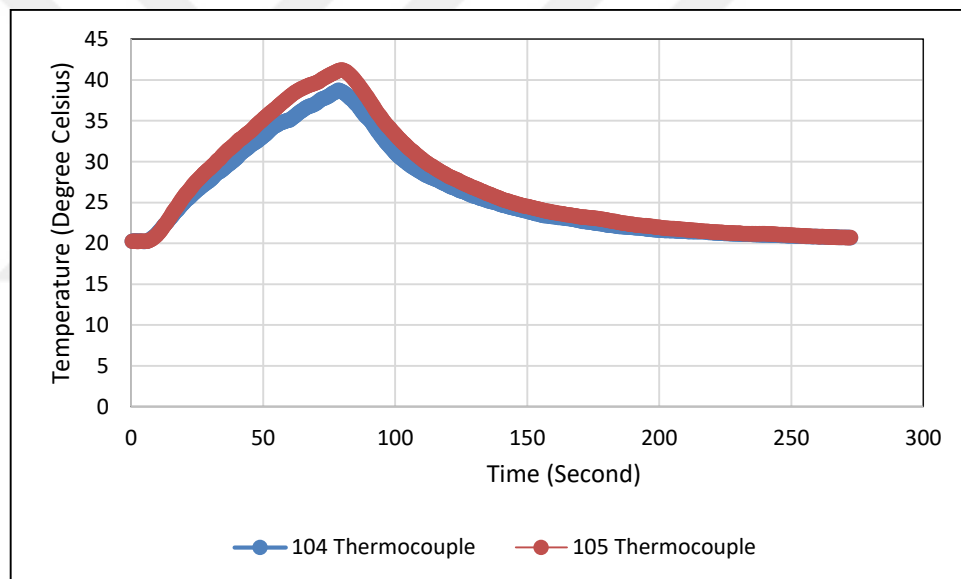


Figure 5.5. Thermocouple measuring shape memory alloy actuation temperature

In Figure 5.5 there are two channels 104 and 105, that means there are two thermocouples are attached to shape memory alloy to observe temperature distribution. 104 is connected to head of the shape memory alloy spring and 105 is connected the end of the shape memory alloy spring. Because of that 104 shows the high temperature. Clearly seen that there is a hysteresis between 50 and 90 seconds and end of the shape memory alloy temperature. It happens because of shape memory alloy material properties changed by heat, austenite to martensite.

5.2. BELLOW COMPRESSION TENSION TEST

In this project, Bellow is used as squid mantle cavity. Mantle cavity which is bellow contains smoke or water in this project. Bellow type mantle cavity is used because of propulsive speciality. Bellow can throw strongly air or water. It can move back and forward and also it has spring constant like a spring. In this project, a specific type bellow is used. Bellow dimensions are shown in Figure 5.6.

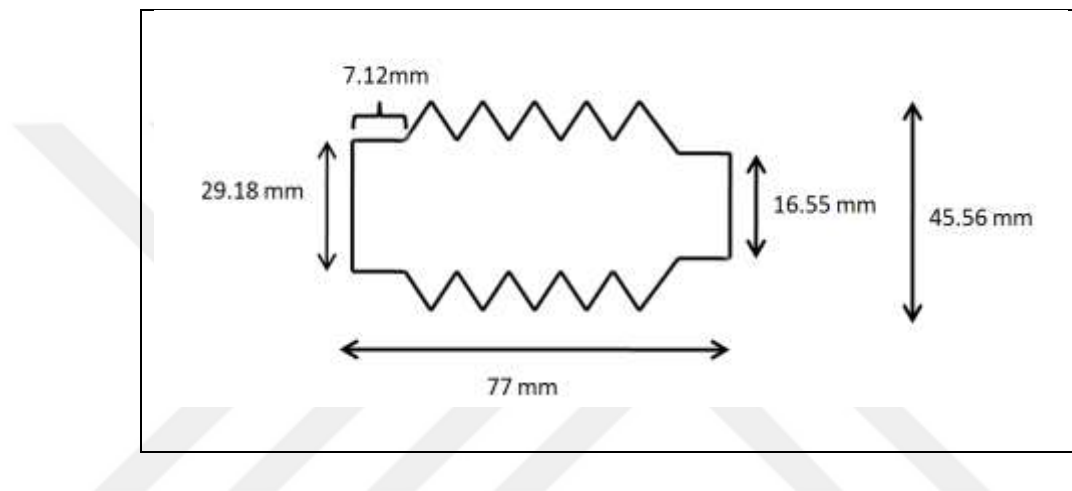


Figure 5.6. Bellow dimensions

Material spring constant can find using spring compression and tension test. In this experiment, spring is compressed and tensioned by using Instron Testing Device. Figure 5.6 there is a bellow drawing figure, which is used as squid mantle wall. This version unlike squid mantle contain smoke instead of water. Bellows have ragged shape therefore, they can behave like springs. Steel springs are used to compress the bellow in order to smoke goes outside and after that, shape memory alloys pulls back bellow to original position and also bellow assits shape memory alloys.



Figure 5.7. Bellow compression by using instron testing device

Bellow behaves like a spring therefore it has a spring constant. In Figure 5.7 bellow is compressed by using Instron machine (Instron 3382J, Norwood, MA, USA) to tensile testing to find bellow spring constant. Instron machine push the specimen with 100 N load cell and data recorded with displacement respect to: 1.0 mm/min.

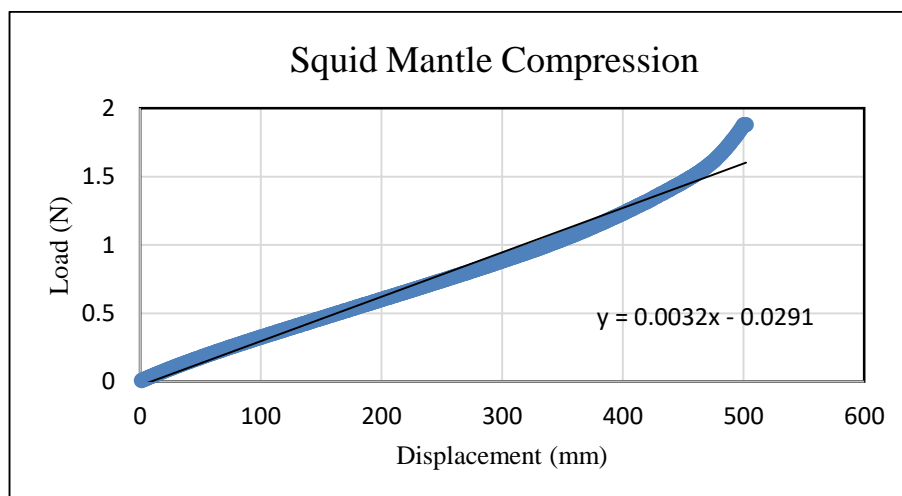


Figure 5.8. Bellow compression and tension graph

Spring constant is found 0.032 N/mm from Load and Displacement graph in Figure 5.8. Tension and Compression test is made from Instron Testing Machine. In this thesis, bellow also acts as a spring. In this reason need to find spring constant.

5.3. SOLENOID WORKING PRINCIPLE

Simple arduino circuit is used to unlock the mechanical squid water propulsion. This solenoid model does not need power supply. With two 150mAh batteries solenoid can be used. Solenoid can be controlled by arduino. In order to run the solenoid needs more power than arduino can supply. I used two batteries, a TIP120 transistor and a diode and a breadboard to connect solenoid to arduino. Solenoid code with arduino is a simple blink code. In this thesis solenoid used as locking system.

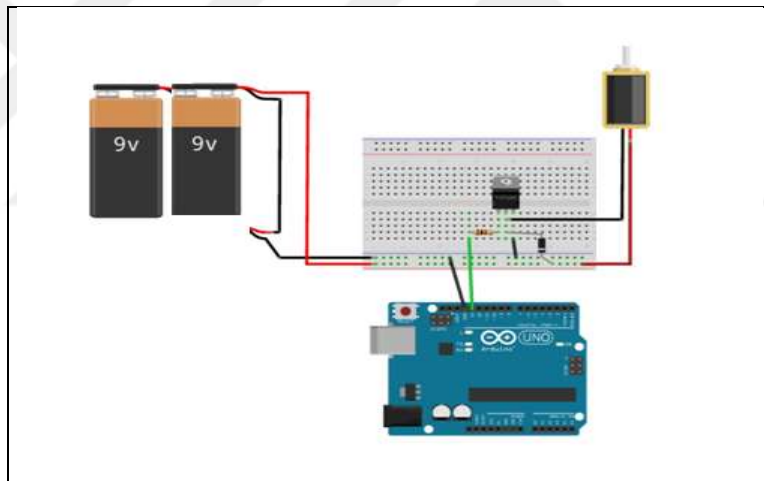


Figure 5.9. Solenoid and Arduino working diagram

Linear solenoids work in two ways such as; back and front. Figure 5.9 shows the solenoid and arduino working diagram. Inside mechanical squid testing device, there is a solenoid. Solenoid's mission is used as a unlock the system. When system is unlocked, starts smoke propulsion. After propulsion, shape memory alloys are heated to pull the system. When shape memory alloys pull bellow, after 35 mm the system gets locked. After then, cooling fans starts to cool shape memory alloys. Two 9 voltages batteries are used to power the solenoid. There is a diode connected to breadboard which is circuit elements consisting of a combination of two semiconductors that only conduct in one direction.

6. SMOKE VISUALIZATION OF ACTUATOR BASED SQUID DESIGN WITH OR WITHOUT SHAPE MEMORY ALLOY

The mechanical squid propulsion efficiency is found by using equation 6.1, which is time dependent unsteady flow efficiency equation (Moslemi et al 2010). F_T represents the time varying thrust and vehicle speed is V_v . D is nozzle diameter, L is smoke distance during propulsion and U_j is jet speed.

$$\eta(t) = \frac{F_T(t)V_v(t)}{F_T(t)V_v(t) + U_j^2(t)\rho\frac{D(t)}{2}\frac{D(t)}{2}\pi L(t)} \quad (6.1)$$

6.1. SMOKE VISUALIZATION WITHOUT SHAPE MEMORY ALLOY

In this thesis project, smoke generator is used to gain smoke. After smoke is placed in the bellow. Bellow is squeezed just like squid water propulsion after that, smoke velocity is calculated with respect to time. In order to do smoke visualization, matlab image processing method is used. When mechanical squid is thrown out the smoke from the bellow, smoke is recorded by camera. Camera's frame per second is 240. Smoke displacement is found by using the center of mass equation. Smoke propulsion is assumed like a rectangle. First and final smoke displacement points are observed and recorded after that, the middle of the first and final points of smoke is assumed as the smoke final displacement point. After finding smoke displacement with respect to time, velocity is calculated by using Richardson extrapolation.

Table 6.1. Camera settings

Duration	1.3867
Bits per Pixel	24
Frame Rate	240
Height	720
Number of Frame	333
Video Format	RGB24
Width	1280

Three different type nozzle diameter is used. Diameters are 2.5mm, 5mm and 10mm and Three different type spring diameter is used as 0.7 mm, 0.9 mm and 1 mm. Tested for smoke propulsion and propulsion efficiency.

Table 6.2. 2.5 mm nozzle diameter and 0.7 mm spring diameter

Time (10⁻³s)	Thrust (kg/ms²)	Vehicle Velocity (m/s)	Diameter (m)	Smoke Length (m)	Smoke Propulsion (m/s)	Efficiency
4.17	0.01554	0.48	0.0025	0.028	6.96	0.999
8.33	0.0063	0.7	0.005	0.064	8.88	0.978
12.5	0.00714	0.4	0.011	0.09	7.2	0.865
16.67	0.0063	0.7	0.02	0.108	6.2	0.701
20.83	0.00294	0.6	0.04	0.13	6	0.230
25	0.00126	0.7	0.05	0.149	5.52	0.090
29.17	0.00168	0.7	0.057	0.168	5.28	0.089
33.33	0.0021	0.72	0.062	0.184	5	0.098
37.5	0.00126	0.96	0.065	0.201	4.95	0.068
41.67	0.0021	0.96	0.067	0.217	4.8	0.102
45.83	0.00252	0.48	0.075	0.238	4.7	0.049
50	0.00504	0.25	0.082	0.257	4	0.054
54.17	0.00546	0.2	0.085	0.267	2.88	0.079
58.33	0.00798	0.16	0.09	0.272	2.16	0.136
62.5	0.0077	0.13	0.093	0.2835	2.08	0.107
66.67	0.00742	0.1	0.096	0.295	2	0.079

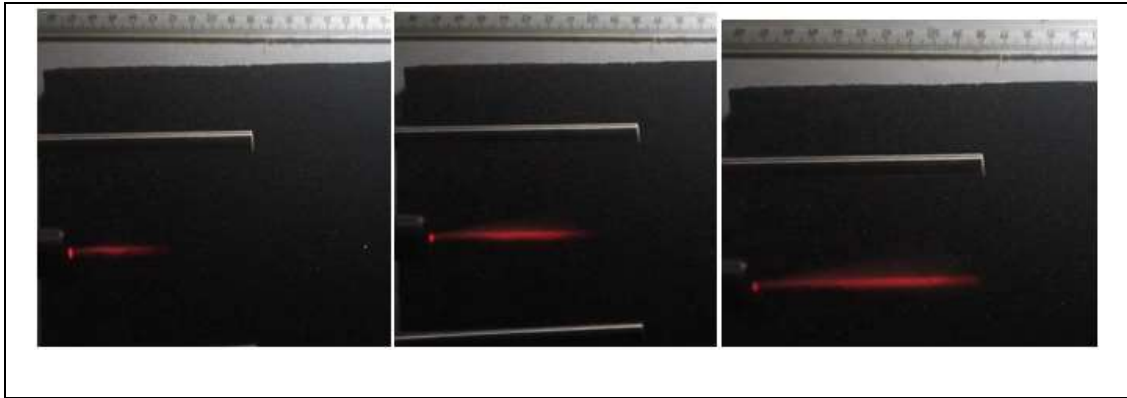


Figure 6.1. Smoke propulsion stages

There are 3 continues frame in Figure 6.1. There is a laser, which is pointed to nozzle exit. When smoke propulsion starts, laser shows smoke location. Ground is fully black and ruler is used to show smoke displacement. These three frames are example of other 16 different frames. Data are shown also in Table 6.2.

Table 6.3. 5mm nozzle diameter and 0.7 mm spring diameter

Time (10⁻³s)	Smoke Length (m)	Vehicle Speed (m/s)	Smoke Propulsion (m/s)	Thrust (kg/ms²)	Diameter (m)	Efficiency
4.167	4.8	0.36	5.16	0.01029	0.005	0.896
8.333	5.88	0.36	6.24	0.00315	0.008	0.795
12.5	5.16	0.6	5.76	0.00189	0.01	0.705
16.66	4.8	0.6	5.4	0.00189	0.022	0.543
20.83	4.08	0.72	4.8	0.0021	0.027	0.526
25	3.6	0.96	4.56	0.00126	0.035	0.338
29.167	3.36	0.72	4.55	0.00126	0.037	0.236
33.333	3.84	0.96	4.65	0.00168	0.04	0.286
37.5	3.36	0.96	4.5	0.0021	0.05	0.238
41.667	2.64	0.96	4.7	0.00378	0.057	0.271
45.833	4.08	0.96	5.04	0.00336	0.06	0.191
50	3.6	1.2	4.8	0.00168	0.075	0.088
54.167	4.08	0.96	4.55	0.00252	0.08	0.094
58.333	3.12	1.2	4.32	0.0021	0.09	0.082
62.5	3.36	0.96	4.32	0.00168	0.095	0.046
66.667	2.64	0.96	3.6	0.00133	0.1	0.046

Table 6.4. 10 mm nozzle diameter and 0.7 mm spring diameter

Time (10 ⁻³ s)	Smoke Displacement (m/s)	Vehicle Speed (m/s)	Smoke Propulsion (m/s)	Thrust (kg/ms ²)	Diameter (m)	Efficiency
4.167	0.026	0.48	4.3	0.0096	0.01	0.5497
8.333	0.042	0.6	5.19	0.00126	0.013	0.0479
12.5	0.0605	0.72	5.16	0.00126	0.02	0.0176
16.667	0.08	0.72	4.7	0.00126	0.023	0.0122
20.833	0.098	0.96	4.3	0.00126	0.03	0.0093
25	0.1077	0.96	4.56	0.00252	0.035	0.0111
29.167	0.125	0.84	4.28	0.00336	0.041	0.0092
33.333	0.1365	0.96	3.72	0.0021	0.055	0.0044
37.5	0.1465	0.96	3.36	0.00126	0.06	0.0025
41.667	0.158	1.2	3.24	0.00252	0.062	0.0060
45.833	0.173	0.96	3	0.00252	0.065	0.0046
50	0.1815	0.84	2.88	0.00168	0.07	0.0024
54.167	0.186	1.2	2.28	0.00189	0.075	0.0052
58.333	0.193	1.08	2.76	0.00231	0.08	0.0033
62.5	0.2042	0.84	2.5	0.00189	0.085	0.0021
66.667	0.215	1.08	2.35	0.00046	0.09	0.0006

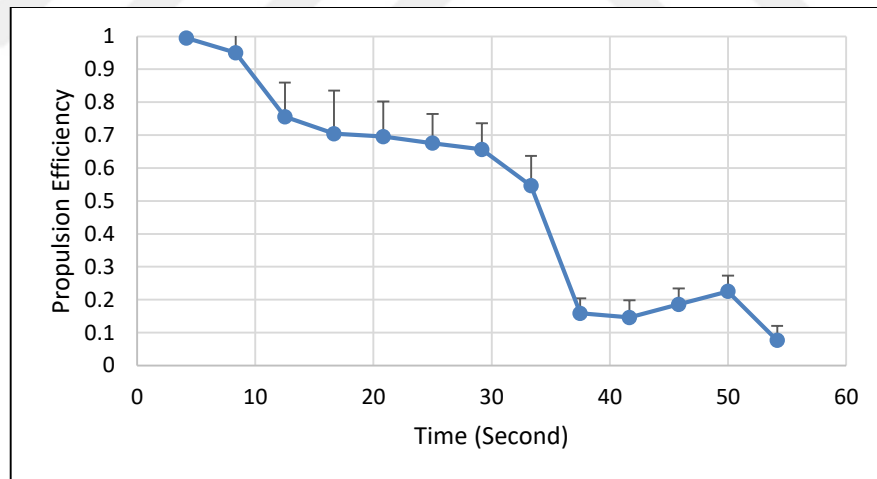


Figure 6.2. Propulsion efficiency versus time 10 mm nozzle diameter 0.7 mm spring diameter

As it can be seen from Figure 6.2 propulsion efficiency drops in 0.01 seconds and efficiency drops faster than 2.5 mm and 5 mm nozzle diameter. Efficiency drops fast and the main reason of this is nozzle diameter dimension. Smoke spreads very comfortably, therefore propulsion efficiency is less than other nozzle diameters. When smoke diffuses to

environment very fast becomes vortexes and smoke displacement gets decrease in time. To keep propulsion efficiency is higher, nozzle diameter must be smaller. Also, Figure 6.2 shows initial propulsion efficiency is less than other nozzle types in same spring diameter comparing with Table 6.2 and Table 6.3's initial propulsion efficiencies.



Figure 6.3. Propulsion stages

Figure 6.3 shows three different frames, which are completely related with each other. Laser is pointed to smoke propulsion location center. When laser makes contact with smoke, smoke can be seen clearly. This method is used motion estimation of smoke and image processing.

Table 6.5. 0.9 mm spring diameter and 2.5 mm nozzle diameter

Time (10 ⁻³ s)	Smoke Displacement (m)	Vehicle Speed (m/s)	Smoke Propulsion (m/s)	Thrust (kg/ms ²)	Diameter (m)	Efficiency
4.167	0.035	0.48	8.88	0.01638	0.0025	0.9994
8.333	0.068	0.48	8.4	0.004585	0.005	0.9864
12.5	0.09	0.96	6.25	0.00378	0.007	0.9882
16.667	0.112	0.96	6.24	0.000245	0.09	0.7270
20.833	0.1335	0.96	6.12	0.00035	0.011	0.6895
25	0.148	1.2	6.2	0.00091	0.025	0.5512
29.167	0.18	1.08	5.76	0.001085	0.05	0.2389
33.333	0.209	1.44	5.94	0.00126	0.07	0.1672
37.5	0.227	1.08	5.4	0.002415	0.085	0.1790
41.667	0.24	1.44	4.56	0.00168	0.09	0.1931
45.833	0.26	1.44	4.44	0.00168	0.1	0.1588
50	0.269	1.44	3.6	0.00231	0.11	0.2397
54.167	0.28	1.44	4.08	0.001365	0.06	0.3190

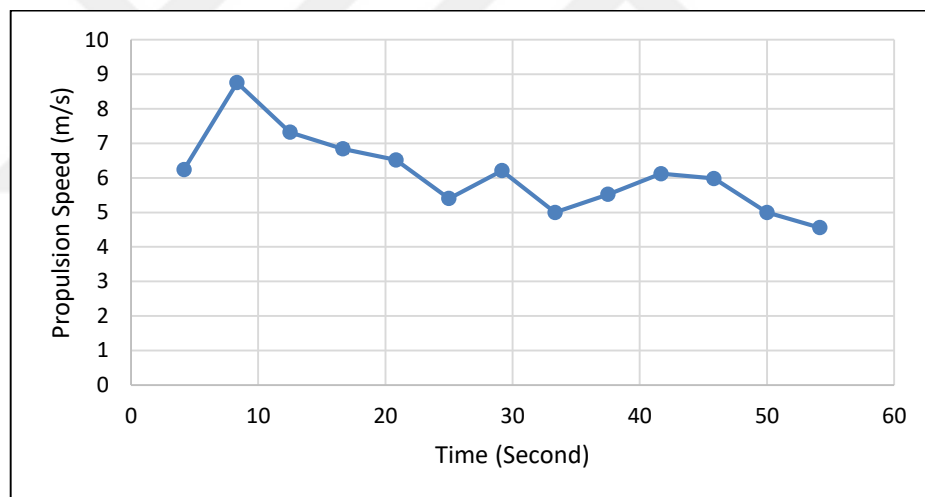


Figure 6.4. Smoke propulsion versus time 2.5 mm nozzle diameter and 0.9 mm spring diameter

Starting propulsion speed is almost 9 m/s (Figure 6.4) and speed does not drop faster than 0.7 mm spring diameter. Fast propulsion happens, because 0.9 mm spring diameter smoke propulsion starts higher speed than 0.7 mm spring diameter because of the spring stiffness. Speed decreases linearly and stable. After a noticeable decrease after 0.01 seconds, it keeps propulsion speed stable at 6 m/s between 0.01 and 0.03 seconds. After propulsion starts, velocity starts to decrease with respect to time. After 0.05 seconds, smoke speed increases,

which unexpected behaviour. This can be happen, because of smoke inside bellow could not distributed homogenousy in bellow. If not distributed homogenousy, remaining smoke make can increase the propulsion speed. It is the main reason of propulsion speed increases.

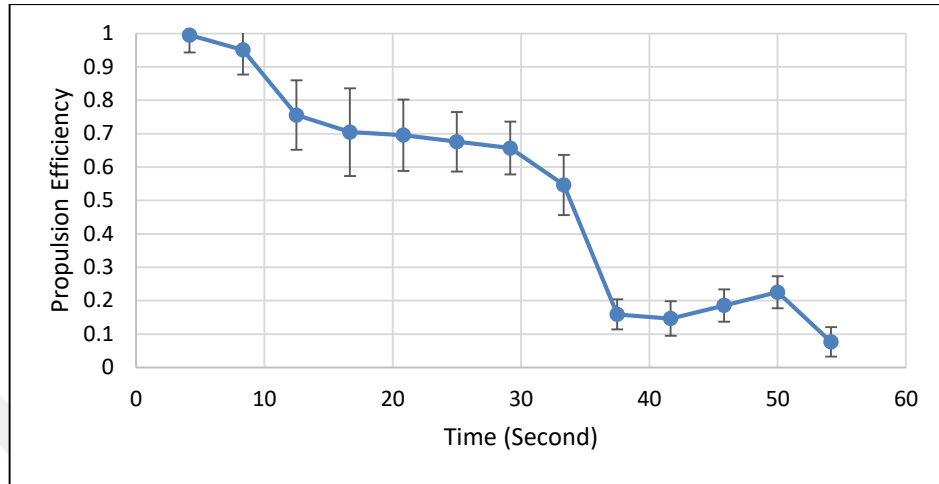


Figure 6.5. Propulsion efficiency versus time 2.5 mm nozzle diameter and 0.9 mm spring diameter

Figure 6.5. shows 0.9 mm spring diameter efficiency does not drop faster than 0.7 mm spring diameter's efficiency and still keeps high efficiency after 0.01 seconds. There is a huge decreases after 0.015 seconds to until 0.03 seconds. It is because of the fast propulsion. Smoke goes outside faster than 0.7 mm spring diameter. Efficiency goes stable after 0.03 second, which is 20 % efficiency. After 0.045 seconds efficiency increases, which is the unexpected result. It happens because of two reasons. While putting smoke in to the bellow, due to the fact that most of the smoke stucks behind in the bellow, during propulsion efficiency increases after a while or image processing data are collected wrong. When comparing with Figure 6.5. and 6.6. shows, when smoke speed is stable propulsion efficiency decreases time between 0.01 and 0.03 seconds, when propulsion speed is decreases propulsion efficiency is get stable time between 0.03 and 0.05 seconds. These results show that, propulsion efficiency change gets speed increasing or decreasing.

Table 6.6. 5mm nozzle diameter and 0.9 mm spring diameter

Time(10^{-3}s)	Smoke Displacement (m)	Vehicle Velocity (m/s)	Smoke Propulsion (m/s)	Thrust (kg/ms²)	Diameter (m)	Efficiency
4.167	0.033	0.36	7.95	0.0231	0.005	0.8556
8.333	0.071	0.72	7.68	0.007385	0.007	0.8346
12.5	0.094	0.7	6.22	0.00301	0.009	0.6265
16.667	0.107	0.72	6.15	0.000665	0.013	0.6265
20.833	0.116	0.96	6.08	0.000595	0.015	0.4299
25	0.127	0.96	5.85	0.00098	0.02	0.4080
29.167	0.146	0.96	5.52	0.001855	0.025	0.4493
33.333	0.161	1.2	5.25	0.00343	0.032	0.4256
37.5	0.183	1.15	5.15	0.002905	0.037	0.3904
41.667	0.202	1.08	5	0.001575	0.04	0.2114
45.833	0.231	0.84	4.25	0.00294	0.045	0.2713
54.167	0.25	0.48	2.76	0.00217	0.051	0.2112
62.5	0.268	0.49	2.65	0.00014	0.06	0.0127
66.667	0.285	0.5	2.67	0.000385	0.07	0.0240
70.833	0.304	0.52	2.87	0.001225	0.084	0.0439
75	0.322	0.58	2.38	0.00105	0.09	0.0498

Table 6.7. 10 mm nozzle diameter and 0.9 mm spring diameter

Time (10 ³ s)	Smoke Displacement (m)	Vehicle Speed (m/s)	Smoke Propulsion (m/s)	Thrust (kg/ms ²)	Diameter (m)	Efficiency
4.167	0.025	0.72	6.72	0.01281	0.01	0.7256
8.333	0.048	0.6	6.12	0.00315	0.017	0.6556
12.5	0.061	0.72	5.65	0.00315	0.021	0.5065
16.667	0.08	0.96	5.52	0.00154	0.035	0.3867
20.833	0.09	0.84	5.24	0.00231	0.04	0.3846
25	0.103	1.08	5	0.00329	0.045	0.1452
29.167	0.118	1.44	5.04	0.00224	0.05	0.1264
33.333	0.13	1.2	4.6	0.001085	0.061	0.1394
37.5	0.141	1.44	4.79	0.000735	0.07	0.0783
41.667	0.155	1.2	4.56	0.00049	0.075	0.0396
45.833	0.172	1.32	4.6	0.000735	0.08	0.0356
50	0.188	1.56	4.98	0.00196	0.084	0.1058
54.167	0.201	1.2	4.24	0.002415	0.089	0.1058
58.333	0.21	1.44	3.6	0.00308	0.095	0.0658
62.5	0.227	2.52	4.72	0.004865	0.1	0.0553
66.667	0.24	0.96	3.06			

Table 6.8. 1mm spring diameter and 2.5 mm nozzle diameter

Time (10 ³ s)	Smoke Displacement (m)	Vehicle Speed (m/s)	Smoke Propulsion (m/s)	Thrust (kg/ms ²)	Diameter (m)	Efficiency
4.166	0.049	1.08	12.84	0.03654	0.0025	0.9989
8.333	0.075	0.84	7.08	0.0168	0.005	0.9947
12.5	0.103	1.2	7.92	0.0315	0.011	0.9840
16.66	0.124	1.2	7.85	0.004463	0.015	0.7987
25	0.15	0.84	7.7	0.01176	0.018	0.8136
29.166	0.174	1.44	7.2	0.01176	0.03	0.7262
33.33	0.201	1.8	8.28	0.00651	0.045	0.3485
37.5	0.229	1.56	8.28	0.00231	0.05	0.1047
41.667	0.253	1.44	7.2	0.00315	0.063	0.0999
45.833	0.274	1.44	6.48	0.00483	0.067	0.1464
50	0.303	1.56	5.56	0.00945	0.075	0.2627
54.16	0.32	1.08	5.16	0.00609	0.082	0.1275
58.33	0.337	0.96	5.04	0.00147	0.09	0.0252
62.5	0.351	0.96	4.32	0.0021	0.095	0.0416

Table 6.9. 1 mm spring diameter and 5 mm nozzle diameter

Time (10 ⁻³ s)	Smoke Displacement (m/s)	Vehicle Speed (m/s)	Smoke Propulsion (m/s)	Thrust (kg/ms ²)	Diameter (m)	Efficiency
4.17	0.048	0.96	10.48	0.02881	0.005	0.9962
8.33	0.078	1.2	8.4	0.0069	0.006	0.9815
12.5	0.103	1.44	8.32	0.00438	0.008	0.9462
16.67	0.133	1.68	8.88	0.00875	0.011	0.9365
20.83	0.175	1.68	8.54	0.00784	0.013	0.8860
25	0.186	2.04	8.25	0.00389	0.015	0.7801
29.17	0.205	2.04	7.8	0.00294	0.02	0.6049
33.33	0.226	2.16	7.2	0.00315	0.025	0.5420
37.5	0.253	1.8	8.28	0.00189	0.03	0.2172
41.67	0.275	2.28	7.56	0.00231	0.035	0.2584
45.83	0.297	1.92	7.2	0.0042	0.04	0.2942
50	0.315	1.92	6.24	0.0042	0.044	0.3019
54.17	0.329	1.44	6.12	0.00252	0.05	0.1304
58.33	0.347	1.44	5.76	0.00462	0.065	0.1483
62.5	0.363	1.44	5.28	0.003252	0.07	0.1073
66.67	0.375	0.24	3.12			

Table 6.10. 10 mm nozzle diameter and 1 mm spring diameter

Time (10 ⁻³ s)	Smoke Displacement (cm/s)	Vehicle Velocity (m/s)	Smoke Propulsion (m/s)	Thrust (kg/ms ²)	Diameter (m)	Efficiency
4.016	0.011	1.2	9	0.00777	0.01	0.9925
8.333	0.042	1.08	8.52	0.0021	0.017	0.8456
12.5	0.07	1.2	7.92	0.00147	0.02	0.8054
16.66	0.092	1.44	7.8	0.00252	0.032	0.4464
20.8	0.117	1.92	7.92	0.00441	0.045	0.4205
25	0.14	2.04	7.56	0.00378	0.05	0.3293
29.16	0.16	1.92	6.72	0.00651	0.066	0.3359
33.333	0.181	1.92	6.96	0.00413	0.073	0.1777
37.5	0.189	1.92	5.72	0.00084	0.085	0.0439
41.66	0.205	2.04	5.88	0.00301	0.09	0.1199
45.83	0.222	2.04	6.04	0.00294	0.095	0.0946
50	0.237	1.92	5.88	0.00357	0.1	0.096
54.16	0.26	1.68	5.38	0.00315	0.106	0.0734
58.333	0.281	1.32	4.9	0.00441	0.109	0.0846
62.5	0.295	1.08	4.44	0.00302	0.115	0.0512
66.666	0.307	0.96	3.84	0.002985	0.12	0.0533
70.833	0.325	0.48	3.19			

6.2. MECHANICAL SQUID MANTLE CAVITY PROPULSION WITH SHAPE MEMORY ALLOY

Mechanic squid has bellow as real squid's mantle cavity. Before smoke visualization experiment, mechanic squid is tested without shape memory alloy in chapter 6.1. When bellow is squeezed by steel spring, smoke propulsion happened. Shape memory alloy is heated to activate. After smoke propulsion, shape memory alloy pulls the bellow to get back original position. SMA is heated with power supply with 5.3 amper and 1.2 volt. After heating, fan works to cool the shape memory alloy. It is small 5V fan, which is enough to cool the SMA wire. Bellow is shown in Figure 5.6 and Figure 5.7.

Table 6.11. SMA actuation observation and records

0.7 mm Spring Diameter	SMA pulling required distance	SMA pulling Total Time	SMA Cooling Time	Going Back Distance	Applied Voltage	Applied Current
2.5 mm Nozzle Diameter	35 mm	7 seconds	30 seconds	15 mm	1 Volt	4.6 Amper
5 mm Nozzle Diameter	35 mm	7 seconds	30 seconds	18 mm	1 Volt	4.6 Amper
10 mm Nozzle Diameter	35 mm	7 seconds	30 seconds	21 mm	1 Volt	4.6 Amper
0.9 mm Spring Diameter	SMA pulling required distance	SMA pulling Total Time	SMA Cooling Time	Going Back Distance	Applied Voltage	Applied Current
2.5 mm Nozzle Diameter	35 mm	9 seconds	30 seconds	28 mm	1 Volt	4.6 Amper
5 mm Nozzle Diameter	35 mm	9 seconds	30 seconds	28 mm	1 Volt	4.6 Amper
10 mm Nozzle Diameter	35 mm	8 seconds	30 seconds	33 mm	1 Volt	4.6 Amper

Table 6.12. 2.5 mm nozzle diameter and 0.7 mm spring diameter with shape memory alloy

Time (10⁻³s)	Smoke Displacement (m)	Vehicle Speed(m/s)	Smoke Propulsion (m/s)	Thrust (kg/ms²)	Diameter (m)	Efficiency
4.2	0.033	0.24	8.16	0.01806	0.0025	0.9975
8.3	0.057	0.24	6	0.00441	0.005	0.9633
12.5	0.079	0.36	5.64	0.00273	0.011	0.8045
16.7	0.096	0.36	4.44	0.00231	0.02	0.5832
20.8	0.112	0.48	4.32	0.00028	0.04	0.0487
25	0.133	0.96	4.28	0.00035	0.05	0.0656
29.2	0.154	0.6	4.12	0.00098	0.057	0.0810
33.3	0.1665	0.72	3.72	0.001575	0.062	0.1402
37.5	0.184	0.48	4.22	0.000998	0.065	0.0419
41.7	0.19	0.48	4.15	0.00021	0.067	0.0086
45.8	0.199	0.48	4.2	0.000438	0.075	0.0133
50	0.224	0.6	4.4	0.000455	0.082	0.0011
54.2	0.244	0.72	4.34	0.00028	0.085	0.0076
58.3	0.2605	0.48	4.44	0.001855	0.09	0.0265
62.5	0.273	0.48	3.48	0.00231	0.093	0.0470
66.7	0.285	0.24	3.12	0.00105	0.096	0.0123
70.8	0.296	0.24	2.88	0.00126	0.100	0.0105
75	0.307	0.72	3.36	0.00147	0.105	0.07974
79.2	0.3205	0.48	3.72	0.00105	0.111	0.0286
83.3	0.33	0.24	2.52	0.00126	0.115	0.0116
87.5	0.342	0.12	3	0.00105	0.12	0.00322

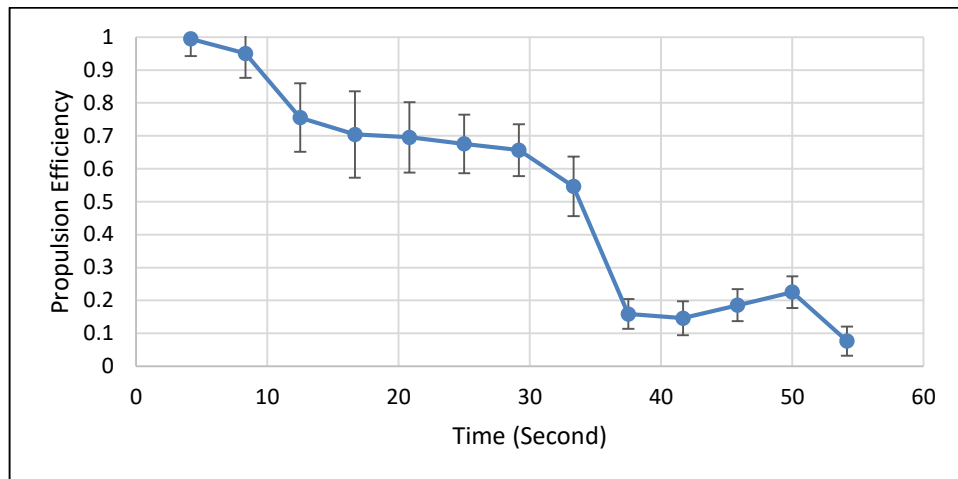


Figure 6.6. Propulsion efficiency of 2.5 mm nozzle diameter and 0.7 mm spring diameter versus time

Propulsion efficiency drops fast in 0.02 second to 10 % efficiency in Figure 6.6. After 0.04 second efficiency becomes almost zero. One of the major effect in decreasing speed of propulsion efficiency was nozzle diameter, and another effect is spring diameter. It was also found that besides these two factors smoke diffusion is also very most important on the efficiency. With high pressure, fluid wants to go out from bellow but nozzle diameter is so little than smoke can not go easily outside and diffuses fast. Therefore, propulsion efficiency decreases faster as shown Figure 6.6.

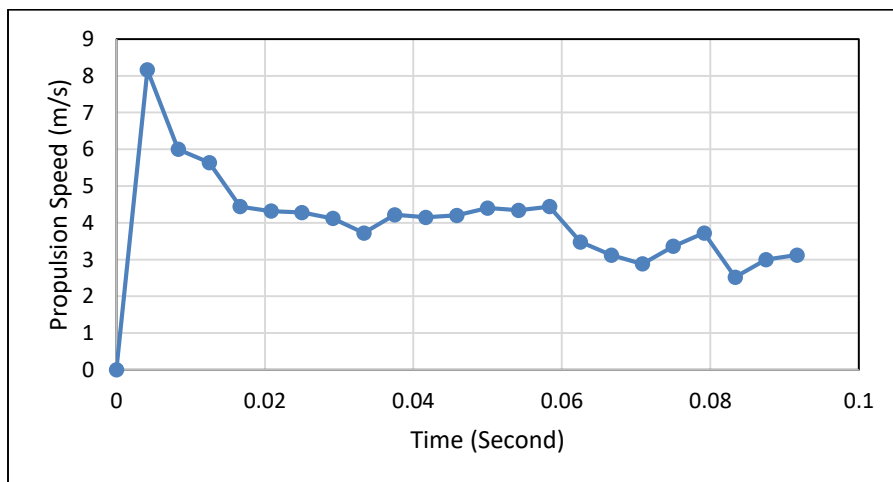


Figure 6.7. Propulsion speed versus time

Propulsion speed starts 8 m/s and after 0.017 seconds keeps steady at 4 m/s during 0.06 seconds. In Figure 6.7 also shows the why propulsion efficiency drops faster. Because after 0.01 seconds, propulsion speed becomes stable, fluid could not flow out easily. Smoke propulsion and propulsion efficiency are not directly proportional. In Figure 6.8. shows after 0.01 seconds propulsion speed is high but propulsion efficiency in Figure 6.7 shows low. Figure 6.7 shows that, after 0.06 seconds speed decreases, but then increases in a while and keeps going with low speed with this instability. Because of the smoke inside bellow could not diffuses equally which means smoke distribution inside bellow is not equal.

Table 6.13. 5 mm nozzle diameter and 0.7 mm spring diameter with shape memory alloy

Time (10 ⁻³ s)	Smoke Displacement (m)	Vehicle Speed (m/s)	Smoke Propulsion (m/s)	Thrust (kg/ms ²)	Diameter	Efficiency
4.167	0.012	0.12	3	0.00945	0.005	0.99813
8.333	0.033	0.36	5.4	0.00546	0.008	0.97600
12.5	0.057	0.36	6	0.00294	0.01	0.86791
16.667	0.077	0.36	5.16	0.00357	0.022	0.62263
20.833	0.092	0.48	4.08	0.00336	0.027	0.61563
25	0.103	0.6	3.24	0.00189	0.035	0.52168
29.167	0.115	0.6	3.48	0.00357	0.037	0.30513
33.333	0.134	0.72	3.28	0.00651	0.04	0.32517
37.5	0.146	0.48	3.36	0.00672	0.05	0.31565
41.667	0.164	0.96	3.45	0.00504	0.057	0.29865
45.833	0.1795	0.6	4.32	0.0021	0.06	0.27564
50	0.1935	0.72	4.08	0.00042	0.075	0.17565
54.167	0.207	0.84	4.08	0.00231	0.08	0.16298
58.333	0.215	0.84	3.15	0.00273	0.09	0.21561
62.5	0.222	0.84	3.78	0.00357	0.095	0.20654
66.667	0.237	0.72	4.32	0.00462	0.1	0.16759
70.833	0.248	0.84	3.48	0.00252	0.105	0.13916
75	0.262	0.72	4.08	0.00112	0.110	0.06066
79.167	0.276	0.72	4.08	0.00133	0.115	0.06996
83.333	0.287	0.72	3.36	0.00252	0.120	0.05255
87.5	0.301	0.6	3.96	0.00231	0.124	0.02546

Table 6.14. 10 mm nozzle diameter and 0.7 mm spring diameter with shape memory alloy

Time (10⁻³s)	Smoke Displacement (m)	Vehicle Speed (m/s)	Smoke Propulsion (m/s)	Thrust (kg/ms²)	Diameter	Efficiency
4.2	0.01	0.24	2.64	0.0099	0.01	0.9976
8.3	0.032	0.36	4.1	0.0082	0.013	0.9763
12.5	0.047	0.36	3.96	0.0031	0.02	0.8289
16.7	0.066	0.36	3.85	0.0006	0.023	0.3582
20.8	0.078	0.72	3.6	0.0011	0.03	0.3056
25	0.09	0.36	3.24	0.0006	0.035	0.1997
29.2	0.101	0.6	3.24	0.0002	0.041	0.0826
33.3	0.111	0.72	3.12	0.0006	0.055	0.1502
37.5	0.122	0.72	3.36	0.0008	0.06	0.1344
41.7	0.132	0.72	3.12	0.0007	0.062	0.1099
45.8	0.146	0.72	3	0.0003	0.065	0.0494
50	0.149	0.84	2.85	0.0006	0.07	0.0969
54.2	0.156	0.72	2.9	0.0018	0.075	0.0856
58.3	0.167	0.96	2	0.0021	0.08	0.0756
62.5	0.177	0.72	2.45	0.0021	0.085	0.0556
66.7	0.184	0.72	2.15	0.0023	0.09	0.0254
70.8	0.193	0.84	2	0.0015	0.01	0.0156
75	0.203	0.84	1.94	0.0021	0.0105	0.0115
79.2	0.2105	0.48	1.82	0.0017	0.0110	0.025
83.3	0.217	0.72	1.92	0.0006	0.0115	0.0477

Table 6.15. 2.5 mm nozzle diameter and 0.9 mm spring diameter with shape memory alloy

Time(10^{-3}s)	Smoke Displacement (m)	Vehicle Speed (m/s)	Smoke Propulsion (m/s)	Thrust (kg/ms^2)	Diameter (m)	Efficiency
4.2	0.014	0.24	10	0.01596	0.0025	0.99820
8.3	0.05	0.48	9.12	0.01281	0.005	0.98690
12.5	0.078	0.6	7.32	0.00483	0.007	0.947442
16.7	0.1015	0.72	6.36	0.0021	0.009	0.852764
20.8	0.13	0.96	6.11	0.00105	0.011	0.686191
25	0.1505	0.84	5.76	0.00119	0.025	0.289789
29.2	0.177	1.08	6.08	0.001855	0.05	0.134962
33.3	0.191	1.08	5.33	0.00154	0.07	0.073806
37.5	0.22	1.2	5.45	0.00175	0.085	0.053624
41.7	0.2345	1.08	4.56	0.001855	0.09	0.060694
45.8	0.254	0.72	4.72	0.00147	0.1	0.023272
50	0.275	0.84	4.04	0.00133	0.11	0.025535
54.2	0.288	0.84	3.96	0.00056	0.120	0.009129
58.3	0.3	0.84	3.72	0.0021	0.125	0.033482
62.5	0.309	0.6	2.76	0.00168	0.130	0.031270
66.7	0.318	0.6	2.76	0.002975	0.138	0.048982
70.8	0.32	0.6	1.08	0.003045	0.140	0.062

Table 6.16. 5 mm nozzle diameter and 0.9 mm spring diameter with shape memory alloy

Time (10 ⁻³ s)	Smoke Displacement (m)	Vehicle Speed (m/s)	Smoke Propulsion (m/s)	Thrust (kg/ms ²)	Diameter (m)	Efficiency
4.166	0.015	0.12	3.72	0.01491	0.005	0.9977
8.333	0.048	0.6	8.52	0.01176	0.007	0.9813
12.5	0.0725	0.72	6.6	0.00462	0.009	0.9430
16.666	0.0945	0.6	5.88	0.00147	0.013	0.6704
20.833	0.108	0.96	5.75	0.00042	0.015	0.3899
25	0.129	0.84	5.65	0.000945	0.02	0.3803
29.166	0.154	1.08	5.2	0.002135	0.025	0.3584
33.333	0.168	1.08	4.44	0.0028	0.032	0.3156
37.5	0.185	1.2	5.28	0.00189	0.037	0.2903
41.666	0.2025	1.32	5.52	0.00357	0.04	0.2756
45.833	0.213	1.2	3.72	0.00357	0.045	0.2246
50	0.2225	1.68	3.96	0.001155	0.051	0.2140
54.166	0.241	1.2	3.54	0.00196	0.06	0.2160
58.333	0.264	1.2	4.25	0.00252	0.07	0.1415
62.5	0.279	1.68	3.52	0.001995	0.084	0.1489
66.666	0.289	0.72	3.12	0.000735	0.09	0.0287
70.833	0.299	0.72	3.12	0.000665	0.105	0.0205
75	0.309	0.36	2.76	0.00112	0.112	0.0096
79.166	0.3185	0.12	2.4	0.000875	0.119	0.0023

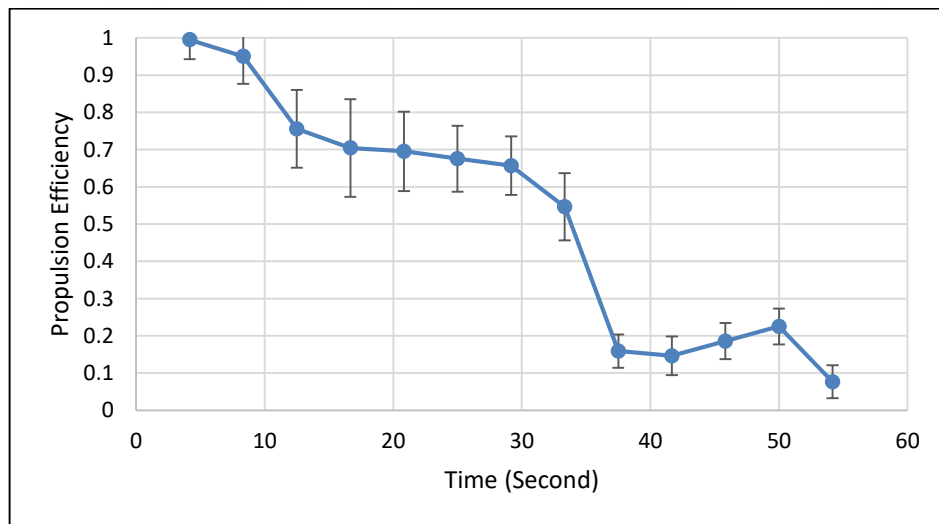


Figure 6.8. 5 mm nozzle diameter and 0.9 mm spring diameter propulsion efficiency versus time

5 mm nozzle diameter efficiency does not drop as fast as 2.5 mm nozzle diameter. Propulsion efficiency drops to 20 % efficiency in 0.02 seconds, after 0.03 seconds later efficiency

becomes 10 %. There is an awkward situation in Figure 6.8. Increasing and decreasing of efficiency step are shown in Figure 6.8. Efficiency increases and decreases are shown in Figure 6.8 between 0.02 and 0.06 seconds and related with efficiency increases and decreases causes from the instability of propulsion speed from Figure 6.9. Propulsion speed instability effects the propulsion efficiency in time.

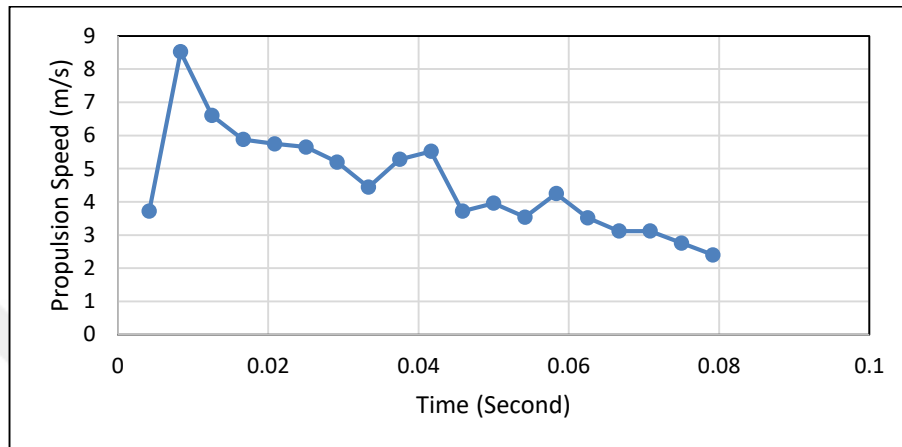


Figure 6.9. 5 mm nozzle diameter and 0.9 mm spring diameter propulsion speed versus time

5 mm nozzle diameter's propulsion speed is slower than the 2.5 mm nozzle diameter. 5 mm nozzle diameter's propulsion speed is decreasing linearly same as 2.5 mm nozzle diameter speed. According to Bernoulli equation, a fluid has reached a narrow section, the speed increases and the pressure drops. From this idea 2.5 mm nozzle diameter has the highest speed than 5 mm nozzle diameter. There is a speed increasing and decreasing between 0.03 and 0.06 second, these anomalies affect the propulsion efficiency and efficiency becomes unstable. It could be affected by the outside air flow speed means that outside air speed is not stable and affecting the propulsion speed, such as air inside dust or little wind can be a resistance to the smoke flow as shown in Figure 6.9.

Table 6.17. 10 mm nozzle diameter and 0.9 mm spring diameter with shape memory alloy

Time (10^{-3} s)	Smoke Displacement (m)	Vehicle Speed (m/s)	Propulsion Speed (m/s)	Thrust (kg/ms^2)	Diameter (m)	Efficiency
4.167	0.0215	0.24	5.4	0.01155	0.01	0.9825
8.333	0.046	0.72	6.6	0.00403	0.017	0.8644
12.5	0.066	0.72	5.5	0.0007	0.021	0.4217
16.667	0.0895	0.96	5.45	0.00098	0.035	0.2690
20.833	0.111	1.32	5.8	0.00095	0.04	0.2100
25	0.1335	1.08	5.6	0.00182	0.045	0.2280
29.167	0.152	1.2	5.25	0.00207	0.05	0.2315
33.333	0.165	1.44	4.56	0.00168	0.061	0.1944
37.5	0.181	1.2	5.04	0.0021	0.07	0.1247
41.667	0.1945	1.32	4.56	0.00147	0.075	0.0980
45.833	0.202	1.32	3.84	0.00063	0.08	0.0526
50	0.212	1.32	3.72	0.00011	0.084	0.0084
54.167	0.2215	1.2	3.48	0.00112	0.089	0.0745
58.333	0.2365	1.08	3.08	0.00168	0.095	0.1024
62.5	0.2425	1.08	2.52	0.00203	0.1	0.1535
66.667	0.2525	0.72	3.12	0.00182	0.107	0.0450
70.833	0.2665	0.48	2.68	0.00105	0.113	0.0194

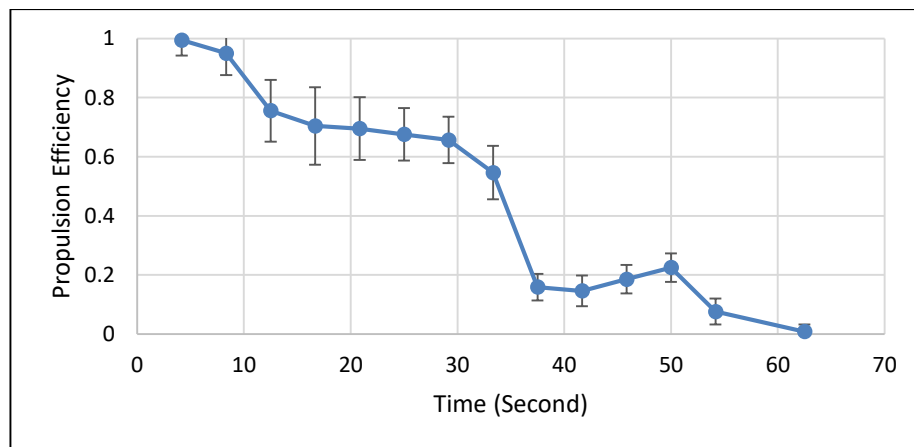


Figure 6.10. 10 mm nozzle diameter and 0.9 mm spring diameter propulsion efficiency versus time

10 mm nozzle diameter has initial propulsion efficiency 100 % unlikely Figure 6.2. Figure 6.2 has 10 mm nozzle diameter but spring diameter is 0.7 mm. This result shows that, spring constant can change propulsion starting efficiency, because of fast propulsion. After 0.01

seconds efficiency drops suddenly, because of smoke propulsion area gets bigger and diffuses easily. Efficiency values becomes 0 % at 0.05 seconds. But after that efficiency increases, believed that bellow inside smoke leftovers goes outside after 0.05 seconds.

Table 6.18. 2.5 mm nozzle diameter and 1 mm spring diameter with shape memory alloy

Time (10⁻³s)	Smoke Displacement (m)	Vehicle Speed (m/s)	Smoke Speed (m/s)	Thrust (kg/ms²)	Diameter (m)	Efficiency
4.1667	0.021	0.48	5.52	0.01659	0.0025	0.9996
8.3333	0.0575	0.72	9.48	0.01029	0.005	0.9864
12.5	0.0875	0.48	7.68	0.00364	0.011	0.7809
16.666	0.1025	1.08	7.52	0.00119	0.015	0.5566
20.833	0.117	0.84	7	0.00098	0.018	0.3608
25	0.142	0.96	6.96	0.00049	0.03	0.0882
29.166	0.161	1.2	6.73	0.001225	0.045	0.1125
33.33	0.189	0.96	6.25	0.0014	0.05	0.0848
37.5	0.2175	0.96	5.94	0.00063	0.063	0.0246
41.666	0.238	0.96	5.88	0.000315	0.067	0.0103
45.83	0.249	0.96	6	0.00154	0.075	0.0360
50	0.2755	0.96	5.25	0.003115	0.082	0.0694
54.166	0.3	0.72	4.21	0.00322	0.09	0.0641
58.333	0.3255	0.48	5	0.00287	0.095	0.0233
62.5	0.341	0.48	4.2	0.00224	0.105	0.0222
66.6667	0.3555	0.24	3.72	0.00126	0.115	0.0063

Table 6.19. 5 mm nozzle diameter and 1 mm spring diameter

Time(10^{-3} s)	Smoke Displacement (m)	Vehicle Speed (m/s)	Propulsion Speed (m/s)	Thrust (kg/ms^2)	Diameter (m)	Efficiency
4.1666	0.025	0.24	6.24	0.01533	0.005	0.9948
8.3333	0.06	0.36	8.76	0.00693	0.006	0.9504
12.5	0.086	1.08	7.32	0.00336	0.008	0.7556
16.666	0.111	0.84	6.84	0.0014	0.011	0.7044
20.8333	0.138	1.2	6.52	0.00252	0.013	0.6954
25	0.1575	0.72	5.4	0.00336	0.015	0.6756
29.166	0.183	1.2	6.21	0.003535	0.02	0.6568
33.3333	0.2105	2.16	5	0.003045	0.025	0.5464
37.5	0.2315	0.48	5.52	0.00196	0.03	0.1588
41.6666	0.252	1.2	6.12	0.001295	0.035	0.1461
45.8333	0.2755	1.44	5.98	0.00196	0.04	0.1857
50	0.297	1.32	5	0.002485	0.044	0.2252
54.166	0.311	1.2	4.56	0.000875	0.05	0.0764
62.5	0.3315	0.6	4.42	0.000315	0.065	0.0087

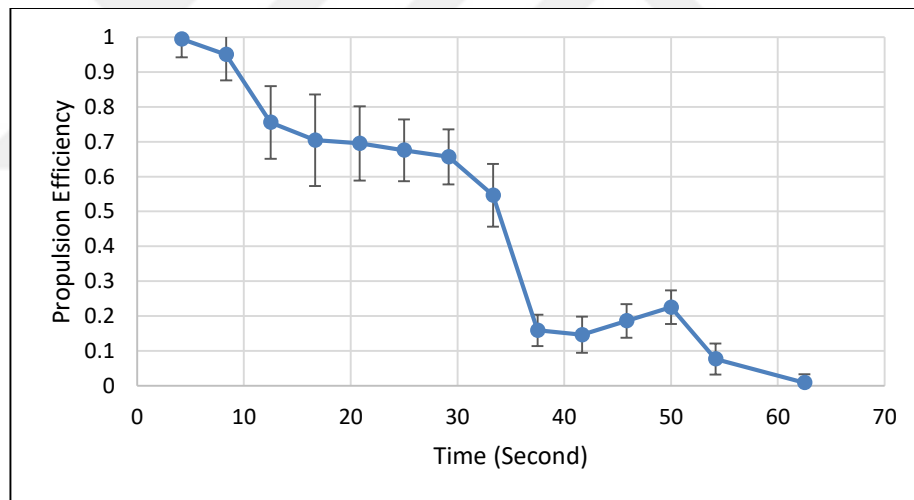


Figure 6.11. Propulsion efficiency of 5 mm diameter and 1 mm spring diameter versus time

Propulsion efficiency unlike 2.5 mm nozzle diameter does not decrease directly. Propulsion efficiency decreases to 30 % in 0.015 seconds after decreasing to 0 % slowly. Figure 6.5. and 6.6. shows, there is a highly relation between smoke speed and propulsion efficiency. Using this hint, using propulsion speed behaviour, propulsion efficiency can be estimated. Which is when smoke speed is stable propulsion efficiency decreases, when propulsion speed is

decreases propulsion speed is get stable. Using Figure 6.11 and Figure 6.12, when smoke speed increases, propulsion efficiency decreases and vice versa.

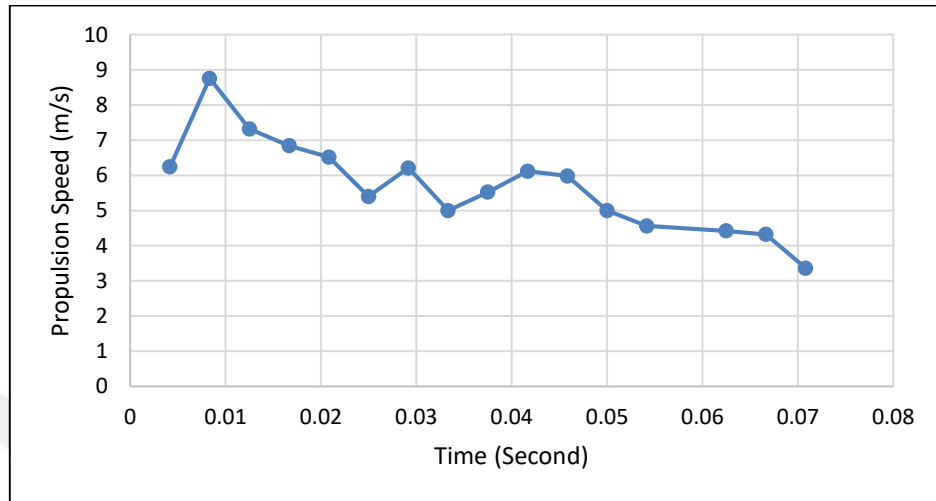


Figure 6.12. Propulsion speed versus time

Initial speed is 6 m/s, that happens because of during image processing record. Speed estimation is made from video records. Video records are splitted to frames by matlab. Smoke displacement is calculated, after smoke passes the nozzle. In this experiment, first frame smoke starts to pass the nozzle and it has less displacement than the next frame. The reason of this the dust or dirt of inside air or inside nozzle, which can create resistance to smoke propulsion. Because of this reason, there is an instability of smoke propulsion speed in Figure 6.12. Maximum propulsion speed is 9 m/s and goes to 3 m/s in 0.07 seconds linearly. After 0.02 second smoke speed increases to 6 m/s and then decreasing to 5. Because of the bellow shape mantle cavity.

Table 6.20. 10 mm nozzle diameter and 1 mm spring diameter

Time (10⁻³s)	Smoke Displacement (m)	Vehicle Speed (m/s)	Propulsion Speed (m/s)	Thrust (kg/ms²)	Diameter (m)	Efficiency
4.167	0.028	0.12	6.84	0.01218	0.01	0.9342
8.333	0.054	0.48	6.72	0.00063	0.017	0.3534
12.5	0.0795	0.36	6.48	0.00063	0.02	0.1778
16.667	0.106	0.24	6.6	0.00126	0.032	0.0753
20.833	0.129	3.48	6	0.00147	0.045	0.1526
25	0.149	0.96	5.76	0.0021	0.05	0.1720
29.167	0.164	1.2	4.8	0.00221	0.066	0.1699
33.333	0.173	1.08	4.5	0.0014	0.073	0.0935
37.5	0.1785	1.32	4	0.00091	0.085	0.0690
41.667	0.1935	1.44	3.98	0.00095	0.09	0.0652
45.833	0.214	1.44	3.45	0.00137	0.095	0.0982
50	0.241	1.44	3.21	0.0013	0.1	0.0873
54.167	0.251	1.32	3.72	0.00259	0.106	0.1003
58.333	0.257	1.32	2.76	0.00385	0.109	0.2173
62.5	0.277	1.2	4	0.00266	0.115	0.0648
66.667	0.2895	0.72	3.72	0.00112	0.12	0.0174
70.833	0.3015	0.48	3.36	0.00301	0.125	0.0334
75	0.3245	0.216	2	0.00308	0.130	0.0371
79.167	0.3295	0.384	1.584	0.00088	0.135	0.0276

7. RESULTS

7.1. EFFECT OF NOZZLE DIAMETER ON PROPULSION EFFICIENCY

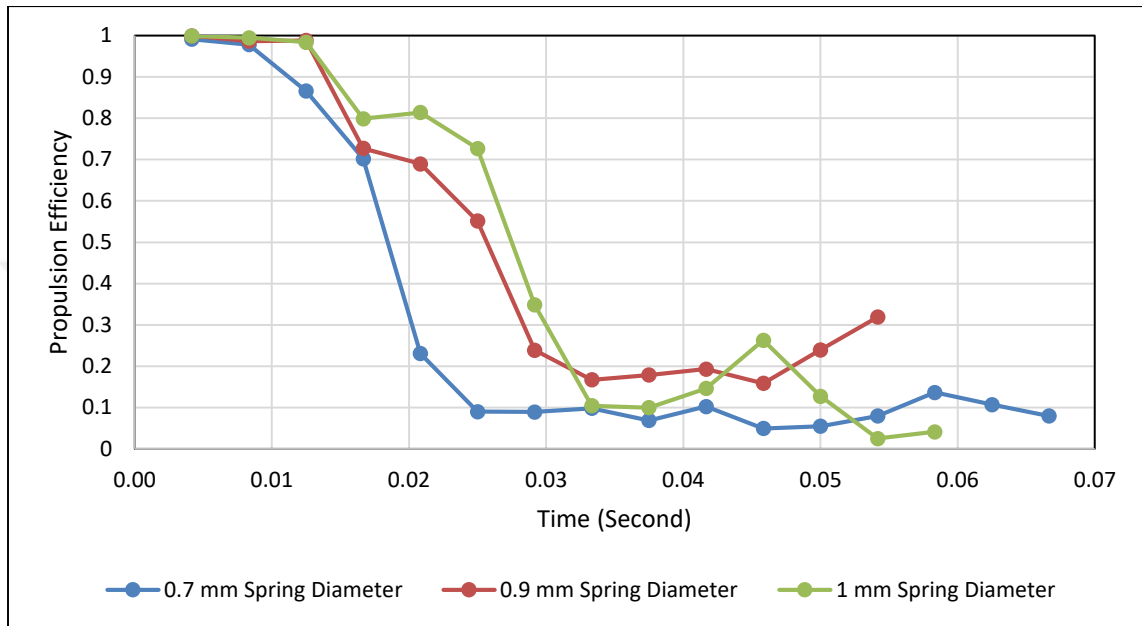


Figure 7.1. Propulsion efficiency versus time on 2.5 mm nozzle diameter with different spring constant

All types of springs have the same starting propulsion efficiency (Figure 7.1). When spring diameter gets higher, springs get more stiffer. After all, which spring has the highest spring diameter, creates more speed for propulsion. But highest speed makes the smoke flows out fast and creates pressure inside bellow. When there is a high pressure in bellow, smoke wants to go out smoothly. If nozzle diameter is small and there is a high pressure in bellow smoke can not flow outside easily, therefore this creates that less efficiency. Because of that reason, all initial propulsion efficiencies are same. After a little time, pressure becomes more balances inside of bellow and propulsion efficiency of 1 mm spring diameter becomes highest.

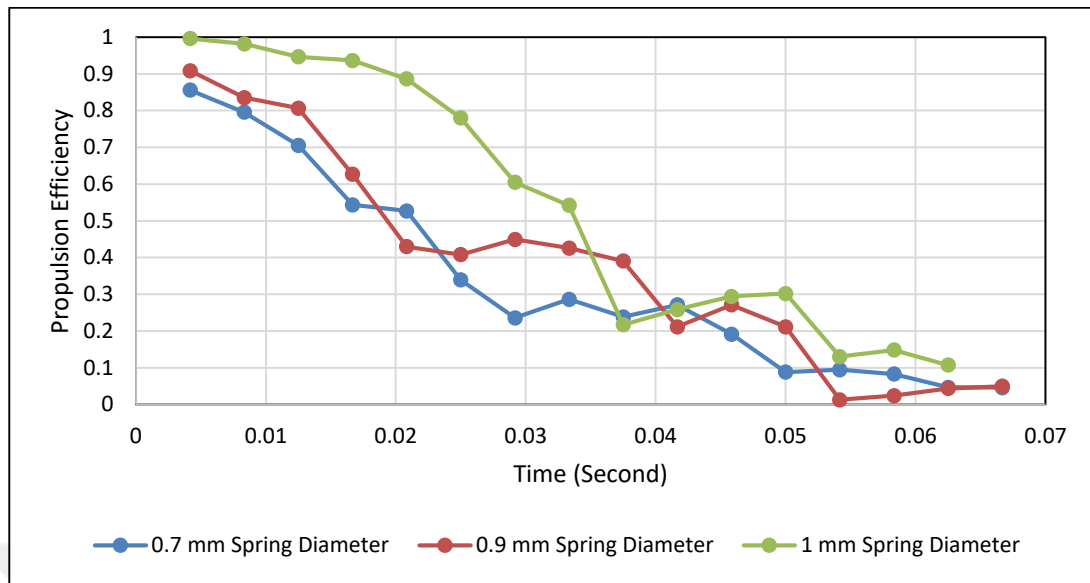


Figure 7.2. Propulsion efficiency versus time on 5 mm nozzle diameter with different spring constant

According to spring diameter types, Figure 7.2 shows reasonable results and shows when nozzle diameter gets bigger, propulsion efficiency drops. 0.9 mm and 0.7 mm spring diameters shows almost same propulsion efficiency. Unlike the 2.5 mm nozzle diameter, smoke can flow out easily in 5 mm nozzle diameter, because of nozzle dimension. There is a huge decrease between 0.03 and 0.04 seconds for 1 mm spring diameter and 0.9 mm spring diameter efficiency becomes higher than others. This can be happen, because of smoke diffusion inside bellow. When there is a high pressure inside bellow, efficiency decrease can be seen. When smoke come across with a high pressure inside bellow, smoke can not flow out freely. This issue is handled by nozzle diameter or spring constant. When nozzle diameter gets bigger, smoke can deal with high pressure inside bellow and flows easily.

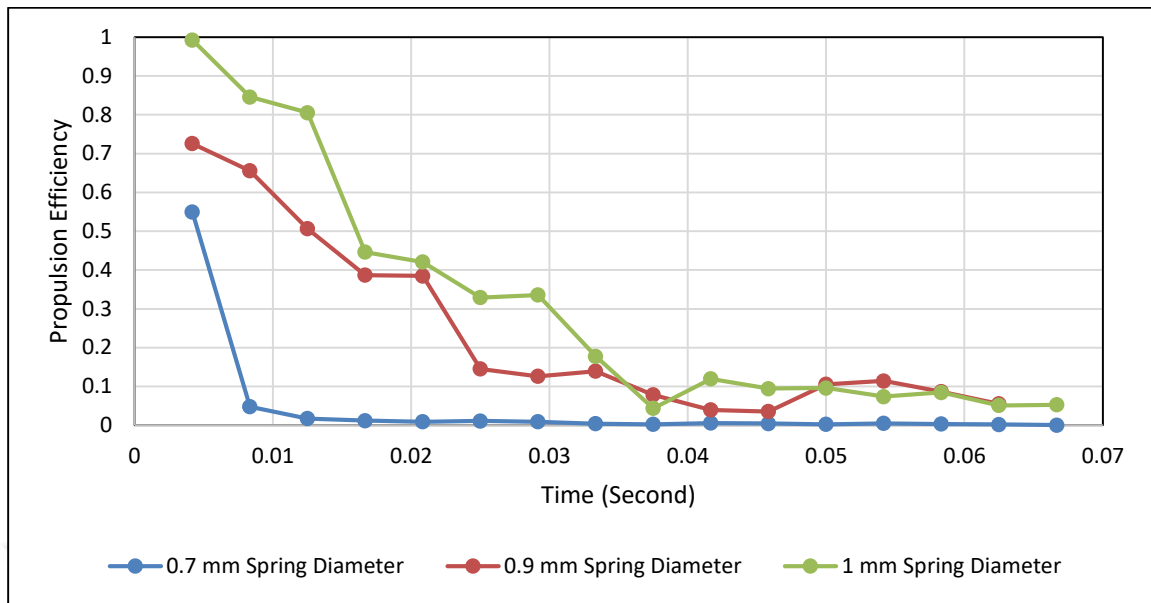


Figure 7.3. Propulsion efficiency versus time on 10 mm nozzle diameter with different spring constant

Figure 7.3 shows using 10 mm nozzle diameter has a visible effect on initial propulsion efficiency. 1 mm spring diameter has higher starting propulsion efficiency than others because of spring diameter. Efficiency behaviour can be estimated by two things. These are smoke speed or nozzle diameter. When nozzle diameter gets wider, smoke starts to diffuse easily and creates vortexes around nozzle exit. But with a high speed, smoke goes straight and it can not diffuse easily. When propulsion happens with low speed, smoke does not flow straight, diffuses everywhere. Which is not good for this experiment.

Table 7.1. Starting propulsion efficiencies

	0.7 mm Spring Diameter	0.9 mm Spring Diameter	1 mm Spring Diameter
2.5 mm Nozzle Diameter	% 99 Propulsion Efficiency	% 99 Propulsion Efficiency	% 99 Propulsion Efficiency
5 mm Nozzle Diameter	% 82 Propulsion Efficiency	% 95 Propulsion Efficiency	% 99 Propulsion Efficiency
10 mm Nozzle Diameter	% 55 Propulsion Efficiency	% 72 Propulsion Efficiency	% 99 Propulsion Efficiency

Table 7.1 shows propulsion efficiency is highest when small nozzle diameter and high speed. Because smoke goes in a line when it goes fast. Therefore smoke does not diffuse outside quickly and as a result propulsion efficiency gets higher.

7.2. EFFECT OF NOZZLE DIAMETER ON PROPULSION EFFICIENCY

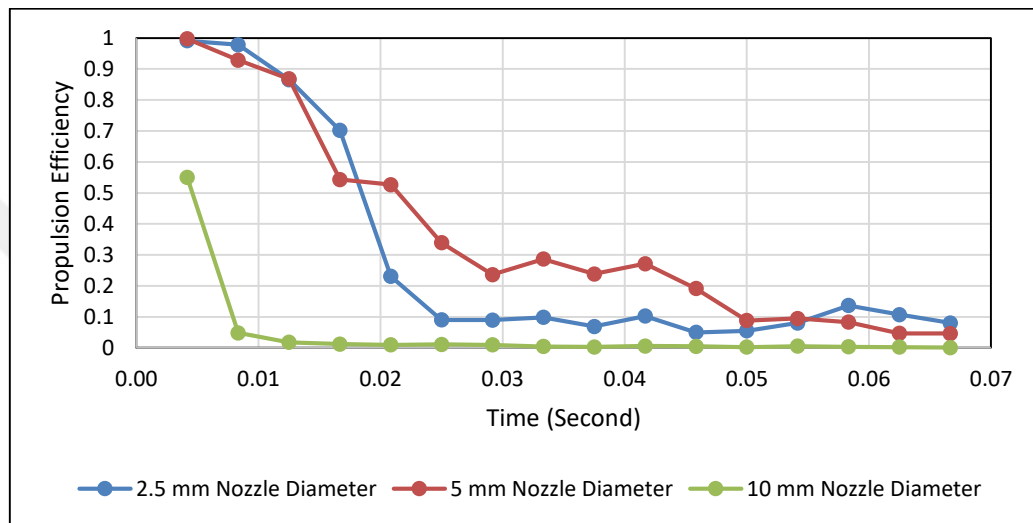


Figure 7.4. Propulsion efficiency versus time on 0.7 mm spring diameter with different nozzle diameter

10 mm nozzle diameter has lowest starting propulsion efficiency and gets almost 0 % in a short time in Figure 7.4. 2.5 mm nozzle diameter has highest efficiency but 5 mm nozzle diameter efficiency gets higher after 0.02 seconds. 2.5 mm and 5 mm nozzle diameter shows same initial propulsion efficiency. This can help to create squid nozzle model. After 0.02 seconds later 5 mm nozzle diameter efficiency is higher than 2.5 mm. This shows that, nozzle diameter is so wide to create straight smoke line. After 0.02 seconds, if smoke nozzle change to 5 mm nozzle diameter, therefore smoke propulsion efficiency keeps higher.

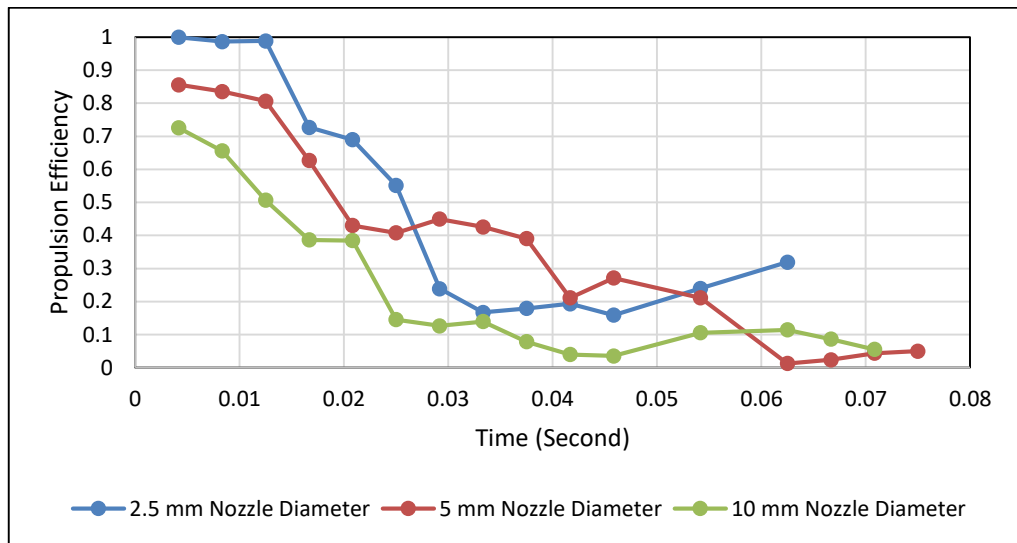


Figure 7.5. Propulsion efficiency versus time on 0.9 mm spring diameter with different nozzle diameter

In 0.9 mm spring diameter, 2.5 mm nozzle diameter initial propulsion efficiency is same as in Figure 7.4. But 5 mm nozzle diameter efficiency becomes lower than in Figure 7.4. During low speed (0.7 mm spring diameter), 2.5 mm and 5 mm nozzle diameter's initial propulsion efficiency becomes same, on medium speed (0.9 mm spring diameter), 5 mm nozzle's initial propulsion efficiency becomes lower. These shows that, 5 mm nozzle is not suitable during medium speed and it can be used for low speed (0.7 mm spring diameter). 10 mm nozzle diameter has the lowest efficiency than others and it is normal because of nozzle diameter.

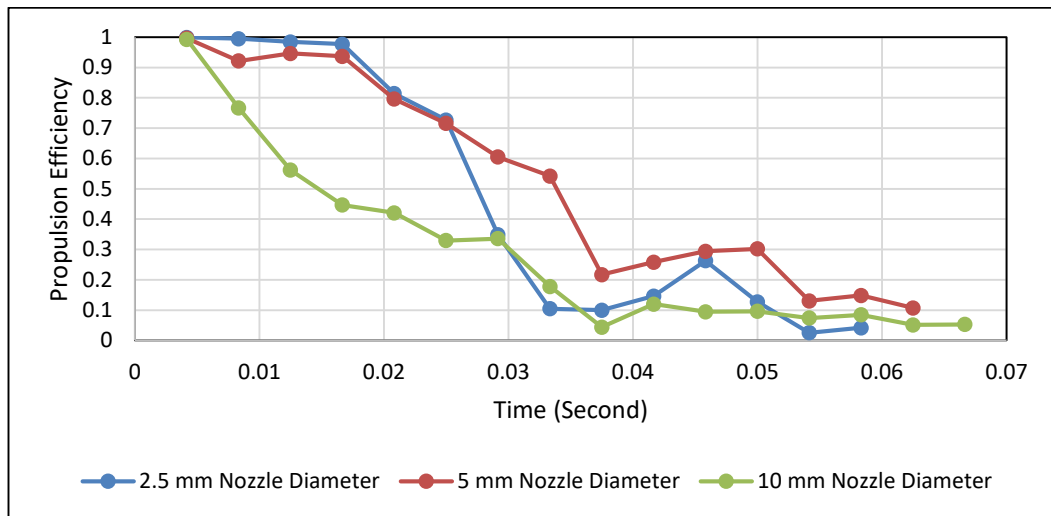


Figure 7.6. Propulsion efficiency versus time on 1 mm spring diameter with different nozzle diameter

10 mm nozzle diameter shows a noticeable change between with 0.9 and 0.7 mm. All starts 100 % efficiency but 5 mm nozzle diameter pass 2.5 mm nozzle diameter after between 0.02 and 0.03 seconds. This nozzle diameter change can be if designed mechanical shape memory alloy spring has 1mm spring diameter to keep propulsion efficiency higher. Unlike the nozzle diameter, spring diameter plays important role to change propulsion efficiencies. For example, in Figure 7.5, 10 mm nozzle diameter's initial propulsion efficiency is 70%, but in Figure 7.6 is 100%. Whatever nozzle diameter is used, propulsion efficiency can be changed by using spring diameter.

7.3. EFFECT OF SPRING CONSTANT ON SMOKE PROPULSION

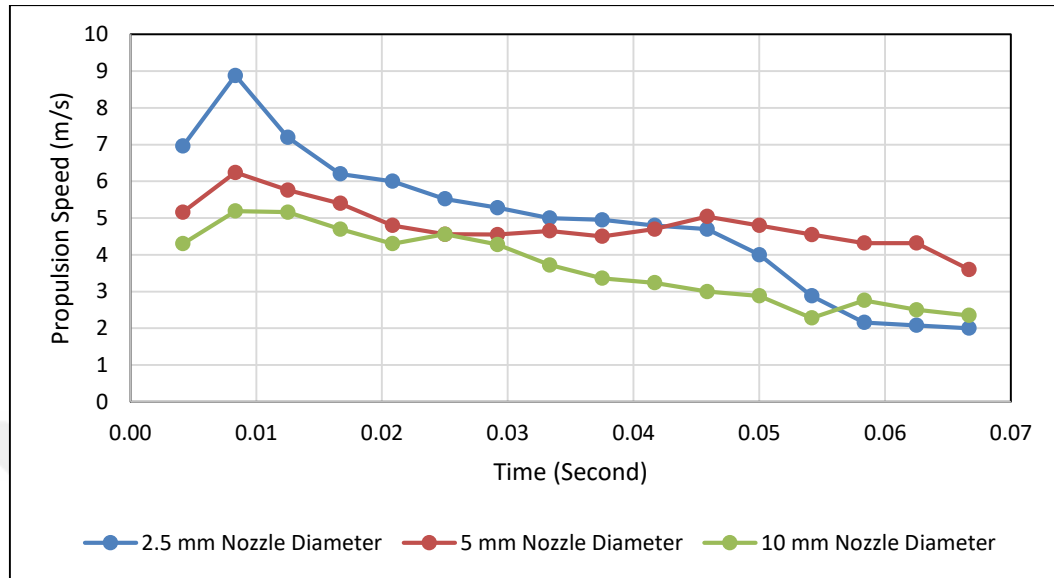


Figure 7.7. Smoke propulsion versus time on 0.7 mm spring diameter with different nozzle diameters

0.7 mm spring graph shows all nozzle diameter have speed increasing after smoke goes out from nozzle in a short time. That happens because of the spring diameter. Spring diameter is not enough to create fast impulse, therefore initial jets become lower. In Figure 7.7 shows that, 5 mm nozzle diameter propulsion starts to increase after 0.03 seconds and passes 2.5 mm nozzle diameter speed. Which can happen because of smoke inside the bellows cannot flow out smoothly for 5 mm nozzle diameter before 0.04 seconds and 5 mm nozzle diameter propulsion speed passes 2.5 mm nozzle diameter propulsion speed after 0.04 seconds. As the propulsion speeds approach 0.07 seconds, 10 mm nozzle diameter speed and 5 mm nozzle diameter become almost the same speed.

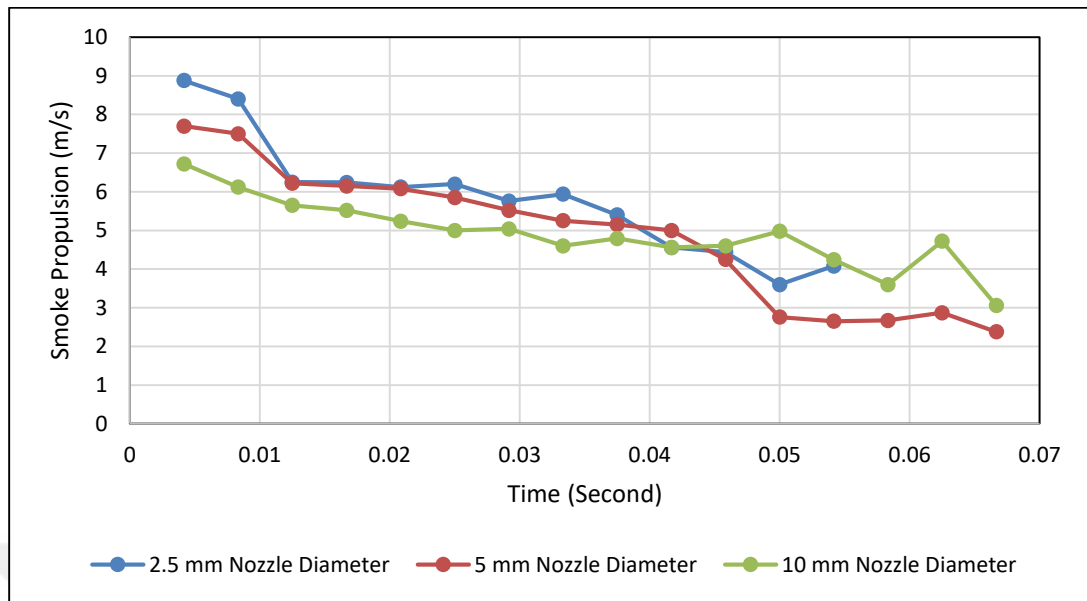


Figure 7.8. Smoke propulsion versus time on 0.9 mm spring diameter with different nozzle diameter

In Figure 7.8, all nozzle diameter's initial propulsion speed is higher than 0.7 mm spring in Figure 7.7 this happens because of the spring stiffness. When spring has more stiffness, creates highest propulsion speed and nozzle diameters become ineffective. After 0.01 seconds 5 mm nozzle and 2.5 mm nozzle propulsion speed gets same in a short time. 10 mm nozzle diameter propulsion speed is lowest, because smoke can go easily and diffuses to outside faster than others. After 0.045 seconds, 5 mm nozzle diameter has the lowest speed in Figure 7.8. This can be happen because, between 0.01 seconds and 0.045 seconds it keeps its speed steable. Which means that, smoke inside bellow flows out smoothly between 0.01 and 0.045 seconds and after 0.045 seconds bellow keeps a little smoke remaining to enough to keep going 2.5 m/s.

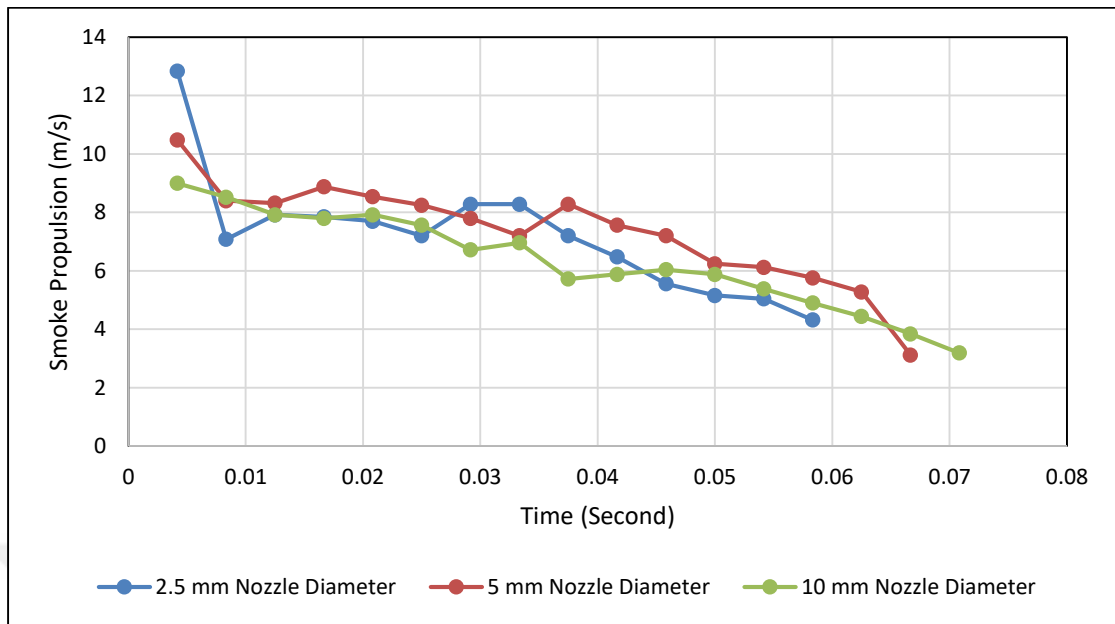


Figure 7.9. Smoke propulsion versus time on 1 mm spring diameter with different nozzle diameter

1 mm spring has the highest propulsion speed but propulsion speed decreases very fast unlike the other Figure 7.7 and Figure 7.8. 2.5 mm nozzle diameter has the highest initial propulsion speed, which happens because of the nozzle diameter dimension. But its speed decreases in a short time, then becomes unstable, such as propulsion speed increases and decreases in time. They shows almost same behaviour during speed observation. Data values are close to each other. They show linear propulsion speed deceleration. During setting smoke inside bellow sometimes smoke flow inside to bellow with different speed. Same situation can be happen for squid in slack water or rough water. This environmental issue can change the squid muscles locomotion. In Figure 2.5 mm nozzle diameter shows unstable behaviour, beucase of this reason. Propulsion speed is increasing and decreasing in time with unbalance speed.

7.4. EFFECT OF NOZZLE DIAMETER PROPULSION EFFICIENCY WITH SHAPE MEMORY ALLOY

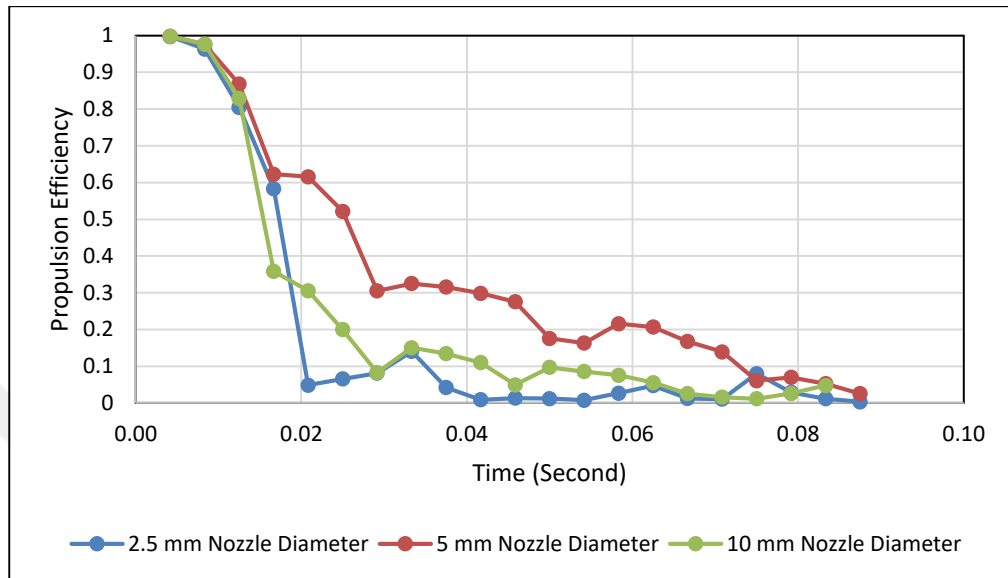


Figure 7.10. Propulsion efficiency of 0.7 mm spring diameter versus time

Using 0.7 mm spring diameter almost every nozzle propulsion efficiency are same until 0.016 seconds, because of nozzle diameter differences. 5 mm nozzle propulsion efficiency gets higher than others. Figure 7.10 shows different results unlike to Figure 7.4. Figure 7.4 has propulsion efficiency versus time in same nozzle diameter and spring constant but in Figure 7.4 there is shape memory alloy. Using shape memory alloy shows different result in propulsion efficiency. Which is happened because of the resistance of shape memory alloy to smoke propulsion. 10 mm nozzle diameter starting propulsion efficiency is 5.5% in Figure 7.4 but in Figure 7.10 initial propulsion efficiency is 100%. Which means that with applying extra resistance to decrease propulsion speed, efficiency can be increased. Also 5 mm nozzle diameter passes 2.5 mm nozzle diameter earlier than figure 7.4.

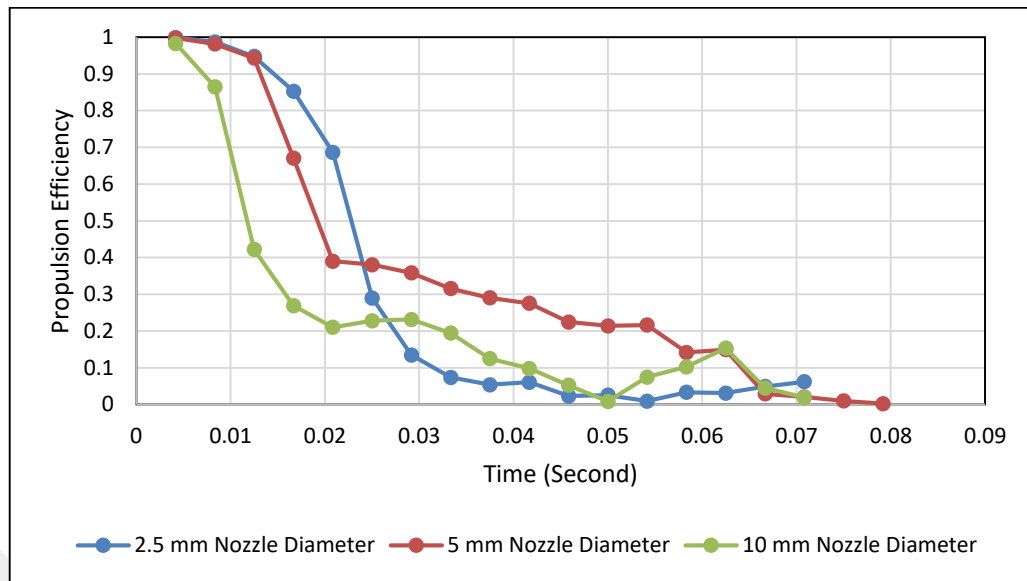


Figure 7.11. Propulsion efficiency of 0.9 mm spring diameter versus time

Unlike the 0.7 mm spring, 2.5 mm nozzle diameter's propulsion efficiency is higher than others until 0.025 seconds. After 0.025 seconds, 5 mm nozzle diameter efficiency does not drop fast and keep linearly decrease in Figure 7.11. 5 mm nozzle diameter's propulsion efficiency becomes higher than 2.5 mm unlikely Figure 7.5. Observing from these results, squids maybe can change their radial muscles length and their nozzle diameter to get optimum propulsion efficiency. In squid propulsion system, radial muscles are used to get water inside mantle. Circular muscles are used for flow propulsion to create jet. Radial muscles and circular muscles are connected to each other and they can create resistance each other during flow propulsion or flow inhale. Because shape memory alloys are used as radial muscles to get flow inside bellow.

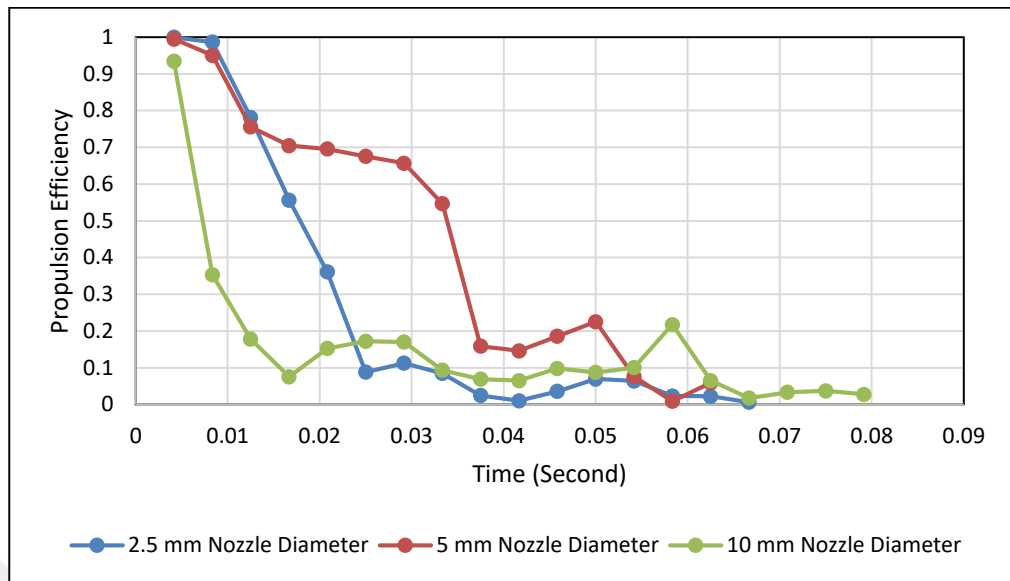


Figure 7.12. Propulsion efficiency of 1 mm spring diameter versus time

1 mm spring diameter has more stiffness than the other spring. Therefore, it has maximum pulling energy. 2.5 mm nozzle does not have high efficiency. Because, smoke can not go through in a tiny way. 5 mm nozzle diameter is the optimum way. In Figure 7.11 and 7.12 shows that, when used a shape memory alloy 5 mm nozzle diameter propulsion efficiency passes 2.5 mm nozzle's efficiency earlier than not used shape memory alloy's propulsion efficiency and 10 mm nozzle diameter initial propulsion efficiency gets higher than not used shape memory alloy's initial propulsion efficiency.

7.5. EFFECT OF SPRING DIAMETER ON PROPULSION EFFICIENCY WITH SHAPE MEMORY ALLOY

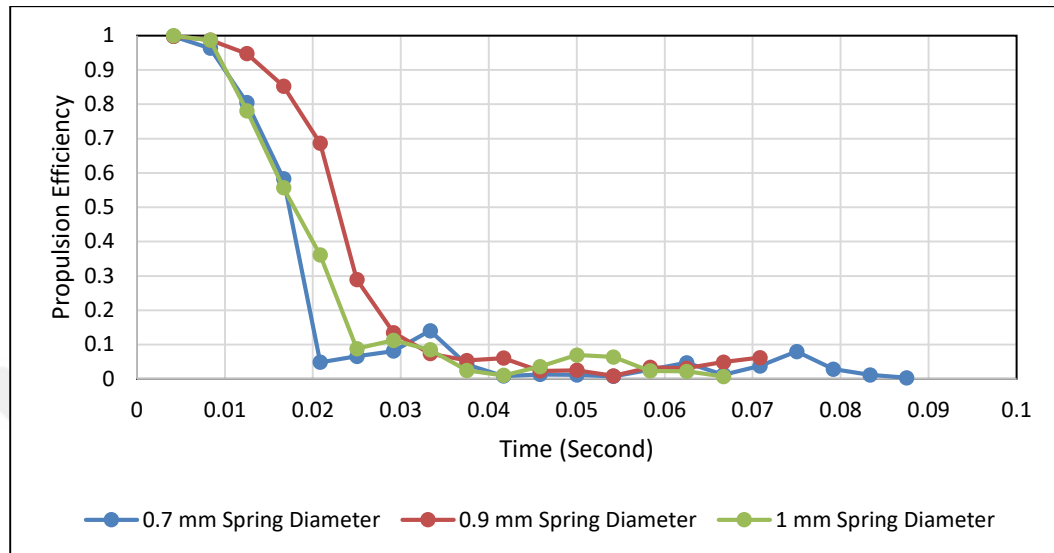


Figure 7.13. Propulsion efficiency of 2.5 mm nozzle diameter versus time

Using 2.5 mm nozzle diameter, 0.9 mm spring gives the efficient propulsion efficiency. But after 0.03 seconds, all springs have almost same propulsion efficiency which is almost 0%. In Figure 7.13, 1 mm spring diameter should have highest propulsion efficiency because of its speed, but 0.9 mm spring diameter's efficiency is highest. Because of nozzle diameter dimension, flow can not goes out easily and create pressure inside bellow when there is a high propulsion speed. This pressure can not let the flow leave the bellow.

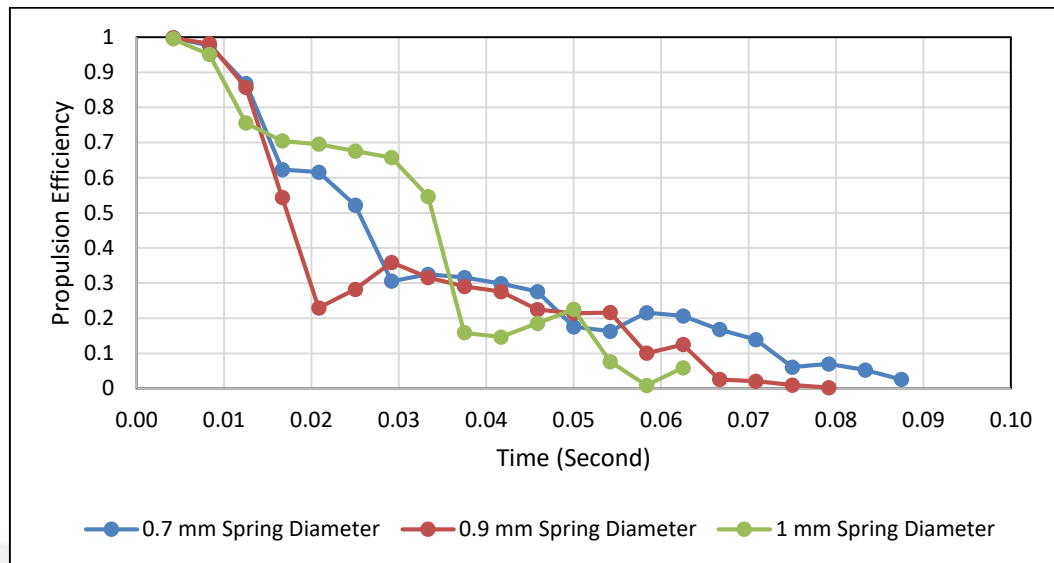


Figure 7.14. Propulsion efficiency of 5 mm nozzle diameter versus time

Using 5 mm nozzle diameter creates a optimum propulsion efficiency to flow way out and 1 mm spring creates fast propulsion than the other springs. Unlike Figure 7.13, 1 mm spring diameter has the highest propulsion efficiency in Figure 7.14. In this efficiency observation, do not need to know 0.05 seconds later, because after 0.05 seconds, smoke propulsion efficiency becomes almost same and propulsion efficiency gets lower 30%. When used 5 mm nozzle and 1 mm spring creates the optimum propulsion efficiency in Figure 7.17. In Figure 7.2 used no shape memory alloy and 1 mm spring diameter efficiency is higher than Figure 7.17. This means that using shape memory alloy creates resistance to efficiency and it is not in good way.

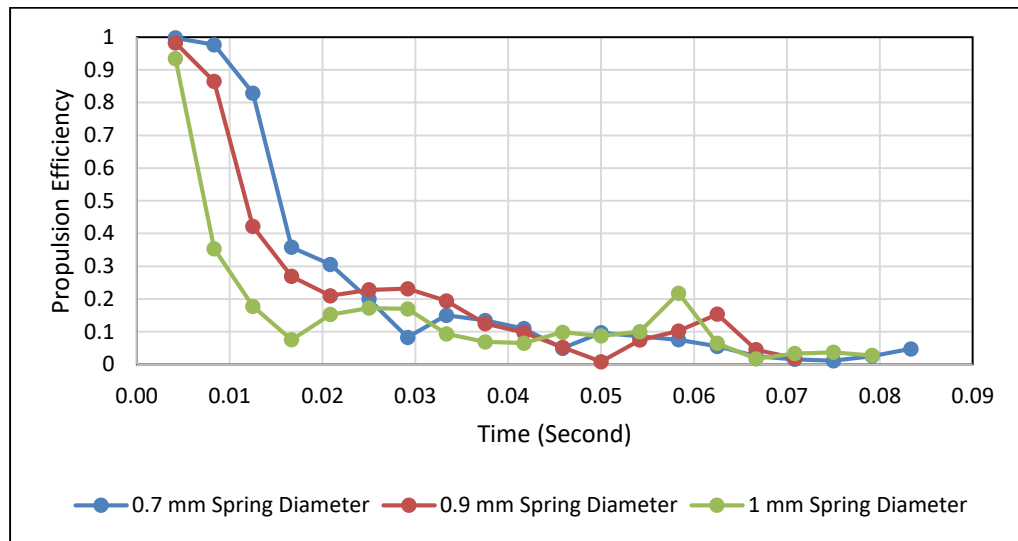


Figure 7.15. Propulsion efficiency of 10 mm nozzle diameter versus time

Surprisingly, 0.7 mm spring has the higher propulsion efficiency. Because low speed makes the smoke goes out slowly and smoke diffuses faster with air therefore propulsion efficiency drops. In Figure 7.15, 0.7 mm spring diameter has propulsion efficiency is highest one except after 0.025 seconds, but in Figure 7.3 there is no used shape memory alloy, which shows 0.7 mm efficiency is the lowest one. Using shape memory alloy also can change the nozzle diameter effect and in this Figure, 0.7 mm spring is the optimum one in propulsion efficiency comparison.

7.6. EFFECT OF NOZZLE DIAMETER ON SMOKE PROPULSION WITH SHAPE MEMORY ALLOY

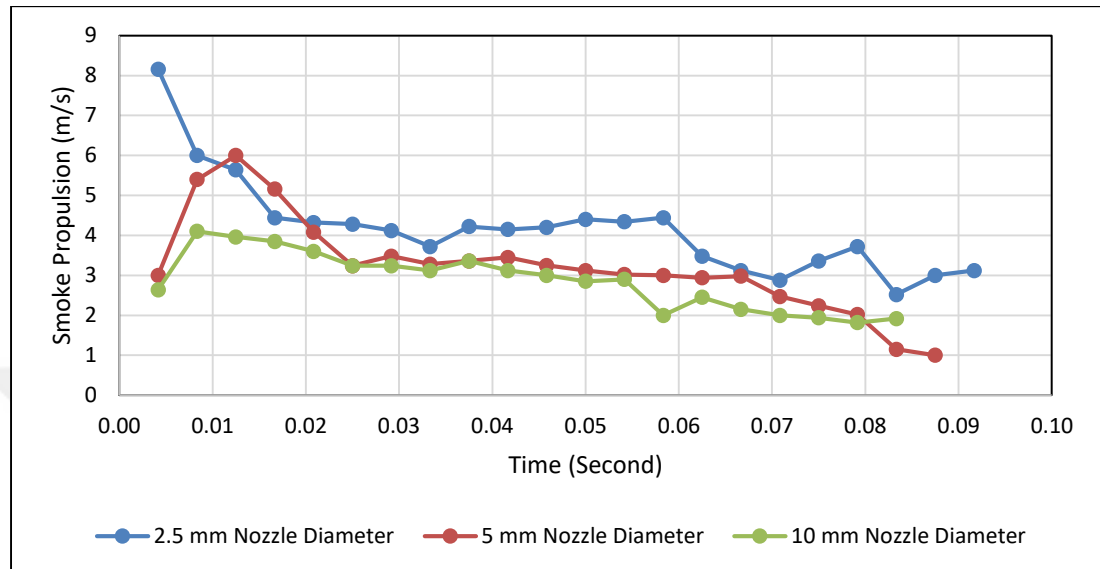


Figure 7.16. Smoke propulsion of 0.7 mm spring diameter versus time

0.7 mm spring diameter has low stiffness than others. Therefore, starting smoke propulsion is lower than the other in Figure 7.16. 10 mm nozzle diameter's smoke propulsion is increased 3 m/s to 4 m/s in a short time and 5 mm nozzle diameter's propulsion speed is also increased 3 m/s to 6 m/s, this is happened because of the smoke distribution is bellow. Which means that, majority of smoke is near to the nozzle and mechanical squid is spend all their smoke in 0.01 seconds. After that second, smoke speeds are decreasing in time but in the mean time, 2.5 mm nozzle diameter speed is decreasing to 0.02 seconds after that it becomes more steable than others.

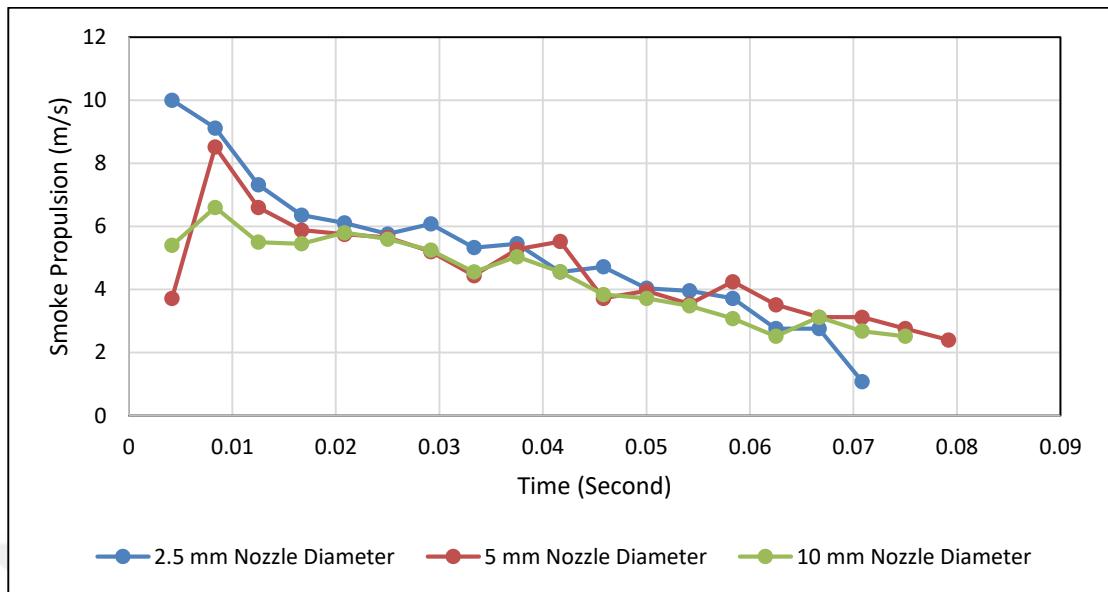


Figure 7.17. Smoke propulsion of 0.9 mm spring diameter

2.5 mm nozzle diameter speed is higher than others in Figure 7.17. It is normal result because, 2.5 mm has tiny nozzle exit to propulsion way out. After a while, smoke propulsion for all nozzle diameter speed becomes equal and decreases linearly. 5 mm nozzle diameter has the lowest initial speed. 10 mm nozzle diameter must have the lowest speed but they are almost equally same speed between 0.02 and 0.06 seconds. It must be because of the same spring constant. In 0.9 mm spring diameter, all nozzle diameter shows same speed activity except initial speeds.

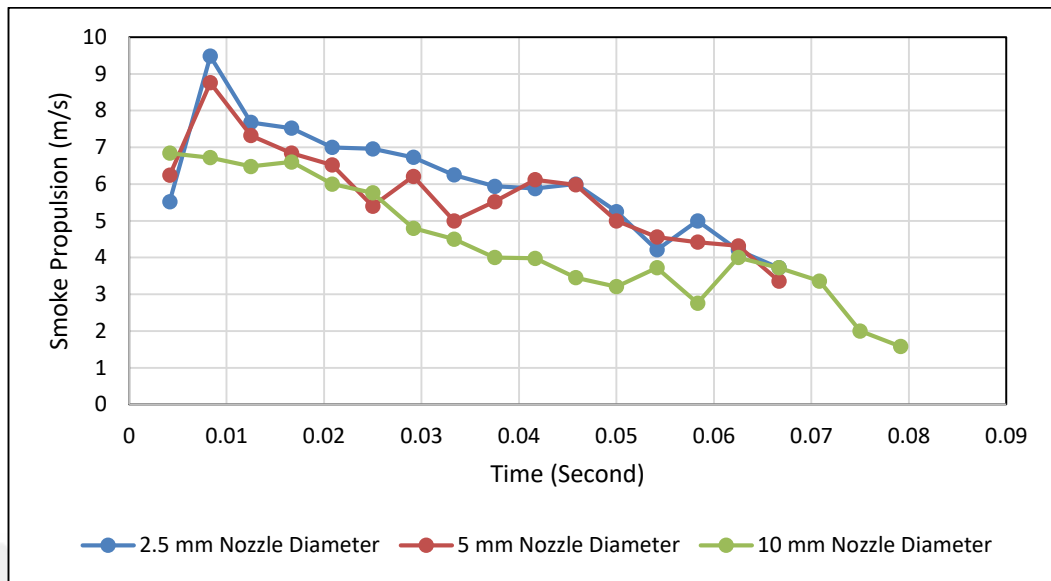


Figure 7.18. Smoke propulsion of 1 mm spring diameter

10 mm nozzle diameter has the lowest propulsion speed because smoke can flow out easily and 1 mm spring diameter has the highest stiffness and it creates highest pull to bellows to make smoke propulsion in Figure 7.18. Which means that, all nozzle diameter has the highest speed than the other spring diameters' propulsion speed. 2.5 mm and 5 mm nozzle starting propulsion speeds show same behaviour. Unlike the 10 mm nozzle diameter, because 10 mm nozzle diameter can not reach them.

7.7. EFFECT OF SPRING DIAMETER ON SMOKE PROPULSION WITH SHAPE MEMORY ALLOY

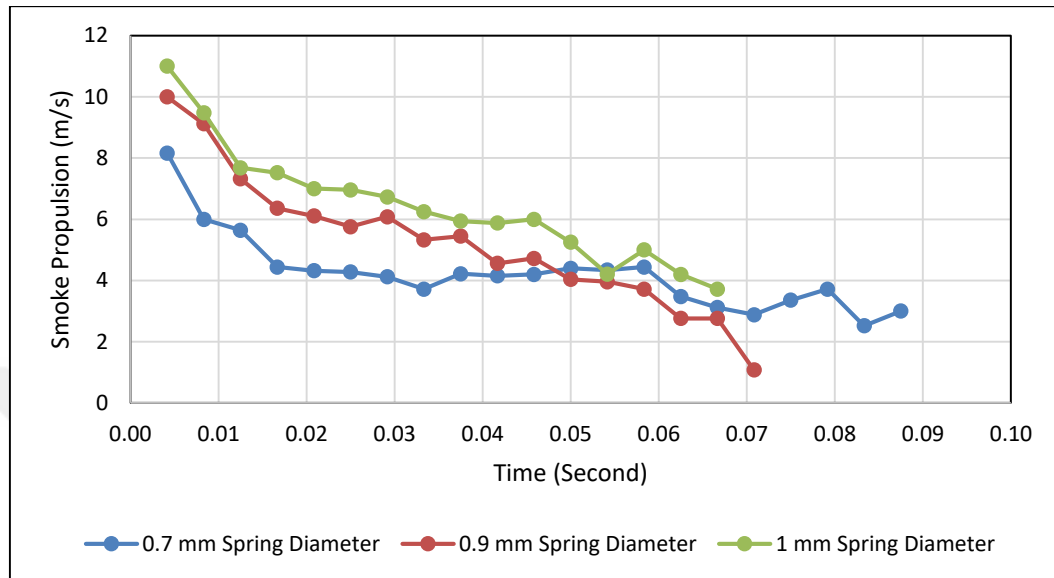


Figure 7.19. Smoke propulsion of 2.5 mm nozzle diameter versus time

1 mm spring diameter has the highest propulsion speed. Because, it has the stiffest spring than the others because of the spring diameter. 1 mm and 0.9 mm spring diameters show decreasing propulsion speed behaviour. Unlikely 0.7 mm spring diameter shows propulsion decrease till 0.02 seconds after then, keep stable propulsion speed. Which means that bellow can hold enough smoke to keep smoke velocity stable in Figure 7.19. After 0.07 seconds, there is no left smoke inside bellow but in 0.7 mm spring diameter has smoke inside bellow. The reason of this, propulsion speed is lower than the others.

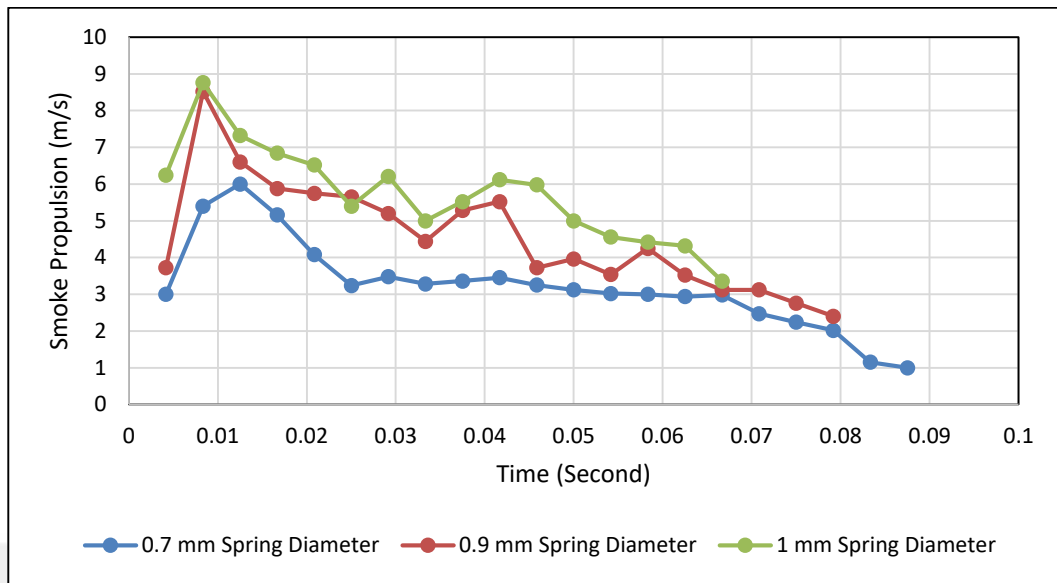


Figure 7.20. Smoke propulsion of 5 mm nozzle diameter versus time

0.9 mm and 1 mm spring diameters gets same maximum speed at the same time but, 0.9 mm spring's speed drops faster than 1 mm spring diameter in Figure 7.20. The reason of this, 0.9 mm spring has the lowest stiffness than 1 mm spring diameter. When a spring get stiffer, it becomes hard to pull becomes stronger. In this propulsion experiment, steel springs are used to create propulsion. When steel springs get more stiffer, creates highest speed to pull the bellow in order to smoke flows out. Also, 0.7 mm spring diameter, has stable speed after 0.025 seconds to 0.065 seconds in Figure 7.20. But in Figure 7.19, 0.7 mm gets stable speed between 0.02 and 0.06 seconds. Which means that, when nozzle diameter is wider, takes time to get speed stable for 0.7 mm spring diameter.

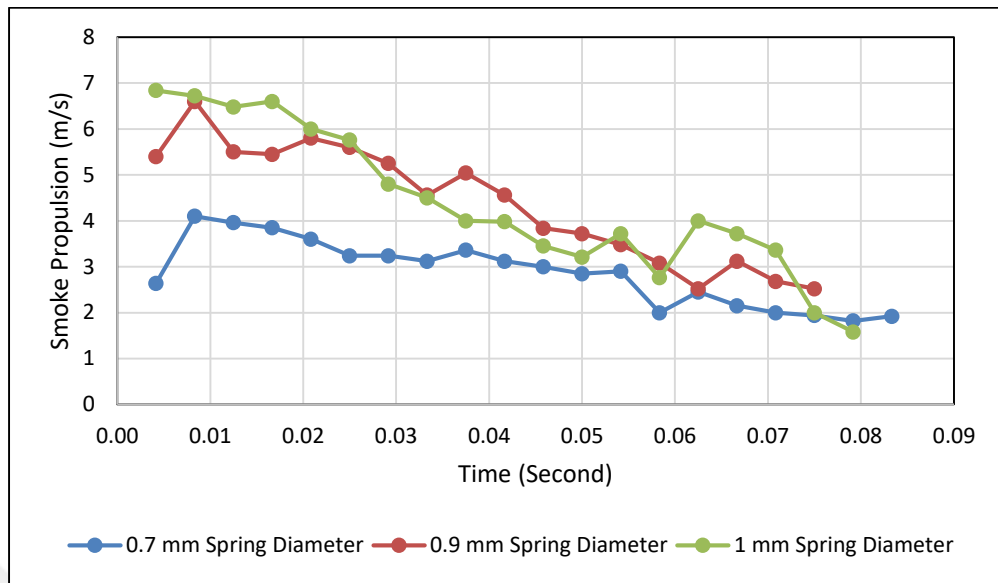


Figure 7.21. Smoke propulsion of 10 mm nozzle diameter versus time

There is a significant difference between and 0.7 mm spring and 0.9 mm spring. All speed are the lowest than other nozzle diameter. When nozzle diameter get wider, propulsion velocity is decreasing. In Figure 7.19 and Figure 7.20 show that nozzle diameter effects the 0.7 mm spring diameter's stable speed. It is also shown in Figure 7.21 and takes more time than the other get the speed stable.

8. CONCLUSION

In this thesis, a mantle wall of a squid was investigated to determine tension, compression and shear behavior of this tissue under the applied load. The results of the tensile test indicated that the mean elastic moduli of the mantle tissue ranged from 500 to 900 kPa. While shear modulus values for the tissue varied from 11 to 15 kPa, constrained and unconstrained compression tests showed that the Poisson's ratio was about 0.34 for the tissue. It was also documented that the circular muscles in a mantle wall occupy about 85-90 percent of the total volume and the radial muscles occupy about 10-15 percent of the total volume based on microscopic tissue analysis. In order to understand the squid propulsion system mechanism created a mechanical squid air in air flow and analyzed to get information about squid nozzle diameter, circular muscles and radial muscles.

Squid mantle wall modeling shows that, squid mantle wall has tiny material structure. Therefore It is very hard to create the real model. In this thesis, also squid mantle wall composite structure is made by mathematical design model. Used shape memory alloy and steel springs as actuators. Shape memory alloys works as a radial muscles. Shape memory alloys pulls the squid mantle wall to take inside water. Steel springs works as circular muscle to make propulsion. Steel spring constant is found both steel and SMA. Steel spring volume over total volume is 40 %. During propulsion over after propulsion, squid mantle wall volume change is 2.5. Also same other propulsion criterias of real squid are used during squid mantle wall composite design, which is made by using squid's mantle cavity diameter and thickness changing by slow swimming and jet escape from Table 5.2.

Squid uses water to escape from its enemies. Mechanical squid uses a bellow as a mantle cavity. Squid uses water in water flow but in this experiment used air in air flow. This mechanical squid uses smoke instead of water. Water propulsion is very hard to observe and inside mechanical squid there are actuator and shape memory alloy heater. Therefore shape memory alloy inside water is hard to heat.

In this thesis the last part is mechanical squid mantle wall analysis with shape memory alloy and without shape memory alloy. Using without shape memory alloy, smoke propulsion speed and propulsion efficiency is higher than the with shape memory alloy. Because shape memory alloy applies resistance to steel spring. Steel spring is used to pull the bellow to

create smoke propulsion and shape memory alloys are used to pull the steel springs therefore SMA acts resistance to steel spring. There is a solenoid to start the propulsion. Smoke is transferred to mechanical squid mantle cavity. After that, jet starts to happen. There is a laser in front of the set up. Shows the smoke location. During jet, camera starts to record. In matlab, camera records turn to frames. Thanks to frames and ruler smoke speed can be calculated. After calculations, smoke propulsion speed and propulsion efficiency is found. Three different nozzle diameter and spring diameter is used. The highest speed and propulsion efficiency is gained from the smallest nozzle diameter and biggest spring diameter as we expected. Bigger nozzle diameter make the smoke diffuse so quick because low speed creates vortexes and this helps to smoke diffuse quickly. Therefore propulsion efficiency becomes smaller when nozzle gets bigger.

5 mm nozzle diameter propulsion efficiency is the second highest. 2.5 mm nozzle diameter has highest starting propulsion efficiency but gets lower than 5 mm nozzle diameter after propulsion and spring diameter has main effect to efficiency drop time. This result is used to observe that squid propulsion nozzle change. Which means that squid changes their nozzle diameter in time during propulsion to get highest speed and efficiency.

Spring diameter has huge effect to propulsion speed. Maximum propulsion speed is from 1 mm spring diameter and 2.5 mm nozzle diameter. This results show that, 2.5 mm nozzle diameter is enough to deal with 1 mm spring diameter. Spring diameter and nozzle diameter plays important role to initial speed but after then propulsion speed get same for each springs and nozzles.

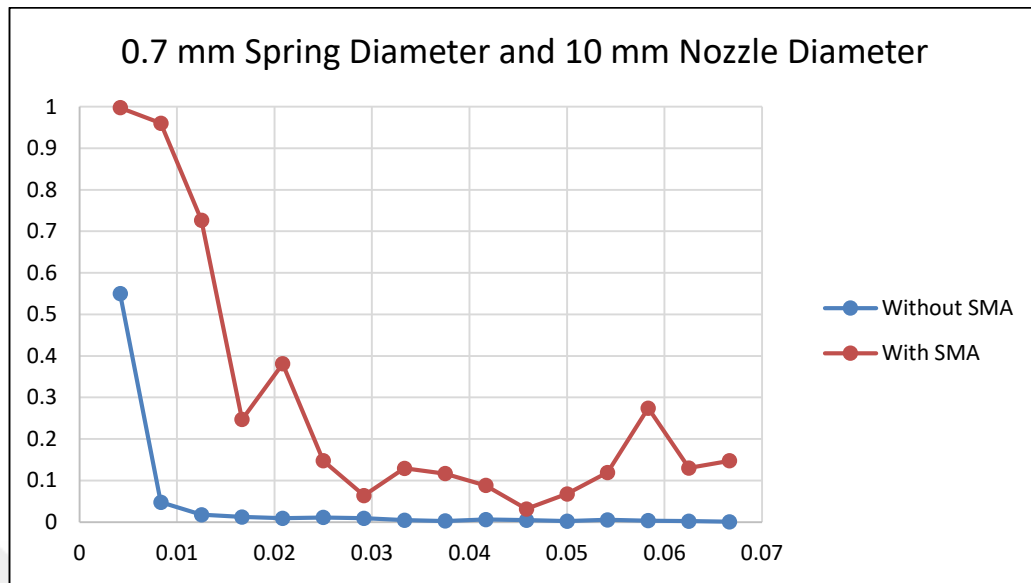


Figure 8.1. Propulsion efficiencies of without and with SMA

Using shape memory alloys or not creates significant effect to propulsion efficiency. They change the behavior of propulsion efficiency. Without SMA, 1 mm spring has the highest propulsion efficiency after 0.9 mm spring for all nozzle dimensions. With SMA, nozzle diameters behavior change all spring's propulsion efficiency. For 2.5 mm nozzle diameter, 0.9 mm spring diameter has the highest propulsion efficiency and after 1 mm spring's propulsion efficiency comes. For 5 mm nozzle diameter $0.9 > 0.7 > 1$ mm spring diameter respectively have the propulsion efficiency. For 10 mm nozzle diameter propulsion efficiency values are $0.7 > 0.9 > 1$ mm spring diameter respectively. In figure 8.1 shows when using SMA in higher nozzle diameter, propulsion efficiency increases. Shape memory alloys effect the propulsion because of the resistance of steel springs.

Smoke propulsion mechanic squid analysis lead a way to water propulsion system design in the future. These results will help to adapt a squid's swimming technique for future studies.

REFERENCES

1. Choon TW, Salleh AS, Jamian S, Ghazali MI. Phase transformation temperatures for shape memory alloy wire. *ENFORMATIKA*. 2007 jan 25; 19:303-7.
2. Shimizu K, and Tadaki T. Shape Memory Alloys, *H. Funakubo, E. D. Gordon and Breach Science Publishers*, 1987.
3. Ruiz LA, Whittlesey RW, Dabiri JO. Vortex-enhanced propulsion. *Journal of Fluid Mechanics*. 2011 Feb;668:5-32.
4. Degeratu S, Bizdoaca NG, Manolea G, Diaconu I, Petrisor A, Degeratu V. On the design of a shape memory alloy spring using thermal analysis. *WSEAS transactions on systems*. 2008 Oct 1;7(10):1006-15.
5. Curtin NA, Woledge RC, Bone Q. Energy storage by passive elastic structures in the mantle of *Sepia officinalis*. *Journal of Experimental Biology*. 2000 Mar 1;203(5):869-78.
6. Gosline JM, Steeves JD, Harman AD, DeMont ME. Patterns of circular and radial mantle muscle activity in respiration and jetting of the squid *Loligo opalescens*. *Journal of Experimental Biology*. 1983 May 1;104(1):97-109.
7. Gosline JM, DeMont ME. Jet propelled swimming in squids. *Sci. Am*. 1985 Jan 1;252(1):96-103.
8. Krieg M, Mohseni K. New perspectives on collagen fibers in the squid mantle. *Journal of morphology*. 2012 Jun 1;273(6):586-95.
9. Kurth JA, Thompson JT, Kier WM. Connective tissue in squid mantle is arranged to accommodate strain gradients. *The Biological Bulletin*. 2014 Aug;227(1):1-6.
10. Macgillivray PS, Anderson EJ, Wright GM, DeMont ME. Structure and mechanics of the squid mantle. *Journal of experimental biology*. 1999 Mar 15;202(6):683-95.

11. Tabatabaei MM, Okbaz A, Olcay AB. Numerical investigation of a longfin inshore squid's flow characteristics. *Ocean Engineering*. 2015 Nov 1;108:462-70.
12. Milligan B, Curin N, Bone QU. Contractile properties of obliquely striated muscle from the mantle of squid (*Alloteuthis subulata*) and cuttlefish (*Sepia officinalis*). *Journal of Experimental Biology*. 1997 Jan 1;200(18):2425-36.
13. Mommsen TP, Ballantyne J, MacDonald D, Gosline J, Hochachka PW. Analogues of red and white muscle in squid mantle. *Proceedings of the National Academy of Sciences*. 1981 May 1;78(5):3274-8.
14. Packard A, Trueman ER. Muscular activity of the mantle of *Sepia* and *Loligo*(Cephalopoda) during respiratory movements and jetting, and its physiological interpretation. *Journal of Experimental Biology*. 1974 Oct 1;61(2):411-9.
15. Staaf DJ, Gilly WF, Denny MW. Aperture effects in squid jet propulsion. *Journal of Experimental Biology*. 2014 May 1;217(9):1588-600.
16. Thompson JT, Bartol IK, Baksi AE, Li KY, Krueger PS. The ontogeny of muscle structure and locomotory function in the long-finned squid *Doryteuthis pealeii*. *Journal of Experimental Biology*. 2010 Apr 1;213(7):1079-91.
17. Thompson JT, Kier WM. Ontogenetic changes in fibrous connective tissue organization in the oval squid, *Sepioteuthis lessoniana* Lesson, 1830. *The Biological Bulletin*. 2001 Oct;201(2):136-53.
18. Thompson JT, Szczepanski JA, Brody J. Mechanical specialization of the obliquely striated circular mantle muscle fibres of the long-finned squid *Doryteuthis pealeii*. *Journal Experimental Biology*. 2008 May 1;211(9):1463-74.

19. Yalcinkaya BH, Erikli Ş, Özilgen BA, Olcay AB, Sorgüven E, Özilgen M. Thermodynamic analysis of the squid mantle muscles and giant axon during slow swimming and jet escape propulsion. *Energy*. 2016 May 1;102537-49.
20. Vogel S. Flow-assisted mantle cavity refilling in jetting squid. *The Biological Bulletin*. 1987 Feb;172(1):61-8.
21. Ward DV, Wainwright SA. Locomotory aspects of squid mantle structure. *Journal of Zoology*. 1972 Aug 1;167(4):437-49.
22. Khan E, Srinivasan SM. A new approach to the design of helical shape memory alloy spring actuators. *Smart Materials Research*. 2011 Dec 26.2011.